UNIVERSITY OF COLOGNE
INSTITUTE OF GEOLOGY AND MINERALOGY

UMEÅ UNIVERSITY
DEPARTMENT OF ECOLOGY AND ENVIRONMENTAL SCIENCE

Diploma Thesis

(Diplomarbeit)

Fourier transform infrared spectroscopy (FTIRS): model development for inferring biogeochemical properties in the 3.6 Ma sediment record of Lake El´gygytgyn, NE Siberia.

---

71 pages
20 figures
4 tables

Presented by

Carsten Meyer-Jacob

October 2010

Supervision:

Prof. Dr. Martin Melles

Dr. Peter Rosén

Erklärung gemäß § 19 Abs. 7 DPO Geologie-Paläontologie

Hiermit erkläre ich, dass die Diplomarbeit von mir selbstständig angefertigt wurde und nur die in der Arbeit erwähnten Hilfsmittel benutzt worden sind.

Köln, Oktober 2010

Carsten Meyer-Jacob

Abstract

This thesis aims to assess quantitatively biogeochemical properties by means of Fourier transform infrared spectroscopy (FTIRS) in the 315 m long and up to 3.6 Ma old sediment record of Lake El´gygytgyn, north-eastern Siberia. FTIRS measurements were performed on 380 sediment samples covering the entire sediment sequence to develop calibration models relating FTIR spectral information and conventional property concentrations by using partial least squares regression (PLSR). Robust calibration models could be established for total carbon (TC), total organic carbon (TOC), total inorganic carbon (TIC), total nitrogen (TN), and biogenic silica (BSi). The external validation of these models yielded a significant correlation between FTIRS-inferred and conventional measured concentrations of $R^2 = 0.90$ for TC, $R^2 = 0.90$ for TOC, $R^2 = 0.89$ for TIC, $R^2 = 0.61$ for TN, and $R^2 = 0.92$ for BSi. An internal calibration including samples from the entire sediment sequence is probably necessary to obtain reliable results from a sediment record of several hundred meters. The application of already existing FTIRS models only based on the uppermost sediments provided considerably poorer correlations between the FTIRS inferred and conventional measured biogeochemical property concentrations. Coefficients of determination of $R^2 = 0.69$ for TC, $R^2 = 0.42$ for TOC, $R^2 = 0.43$ for TN, and $R^2 = 0.84$ for BSi resulted from the external validation. The lower prediction accuracy of these models probably indicates changes of the sediment composition in the deeper parts of the sedimentary record compared to the uppermost sediments. The developed FTIRS models were subsequently applied to FTIR spectra of 677 sediment samples related to the marine isotope stage 11 (MIS 11) to reconstruct past environmental and climatic changes in the Siberian Arctic during this interglacial. The results suggest that the MIS 11 was a particularly pronounced interglacial showing a very high bioproductivity in Lake El´gygytgyn. Its duration in the Siberian Arctic is presumably comparable to its prolonged duration in continental interior Asia (~30 kyr). Furthermore, potential indications for diagenesis induced changes in the sediment composition and the occurrence of carbonates within the sediment record of Lake El´gygytgyn were found by means of FTIRS. The findings of this study confirm the great potential of Fourier transform infrared spectroscopy in paleoclimate research.

Zusammenfassung

Ziel der vorliegenden Arbeit ist die quantitative Bestimmung von biogeochemischen Bestandteilen mittels Fourier-Transform-Infrarotspektroskopie (FTIRS) in der 315 m langen und bis zu 3,6 Mio. Jahre alten Sedimentabfolge des El´gygytgyn-Sees in Nordost-Sibirien. FTIRS-Messungen wurden an 380 über die gesamte Sedimentsequenz verteilte Sedimentproben durchgeführt, um Kalibrationsmodelle zu entwickeln, die FTIR-Spektralinformationen und konventionell gemessene Konzentrationen biogeochemischer Bestandteile durch PLS- (Partial Least Squares) Regressionen in Beziehung setzen. Robuste Kalibrationsmodelle konnten für Gesamtkohlenstoff (TC), organischen Gesamtkohlenstoff (TOC), anorganischen Gesamtkohlenstoff (TIC), Gesamtstickstoff (TN) und biogenes Silikat (BSi) aufgestellt werden. Die externe Validierung dieser Modelle ergab signifikante Korrelationen zwischen den FTIRS und den konventionell gemessen Konzentrationen mit Bestimmtheitsmaßen von R^2 = 0.90 für TC, R^2 = 0.90 für TOC, R^2 = 0.89 für TIC, R^2 = 0.61 für TN und R^2 = 0.92 für BSi. Eine interne Kalibrierung, die Sedimentproben der gesamten Sedimentsequenz enthält, ist wahrscheinlich notwendig, um verlässliche Ergebnisse bei einer Sedimentabfolge von mehreren hundert Metern zu erhalten. Aus der Anwendung von bereits existierenden Kalibrationsmodellen, die nur auf den obersten Sedimenten basieren (16.60 m), ergaben sich bedeutend schlechtere Korrelationen zwischen den FTIRS und den konventionell bestimmten Konzentrationen der biogeochemischen Bestandteile. Bestimmtheitsmaße von R2 = 0,69 für TC, R2 = 0,42 für TOC, R2 = 0.43 für TN und R2 = 0.84 resultierten aus der externen Validierung. Die niedrigere Vorhersagegenauigkeit dieser Modelle deutet wahrscheinlich auf Änderungen der Sedimentzusammensetzung in den tieferen Teilen der sedimentären Abfolge im Vergleich zu den obersten Sedimenten hin. Die entwickelten FTIRS-Modelle wurden anschließend an FTIR-Spektren von 677 Sedimentproben, die dem marinen Isotopenstadium 11 (MIS 11) zugeordnet werden, angewandt, um Änderungen in der Klima- und Umweltgeschichte in der sibirischen Arktis während dieses Interglaziales zu rekonstruieren. Die Ergebnisse lassen darauf schließen, dass das MIS 11 ein besonders ausgeprägtes Interglazial mit einer sehr hohen Bioproduktivität im El´gygytgyn-See war. Seine Dauer in der sibirischen Arktis ist vermutlich vergleichbar mit seiner ausgedehnten Dauer im kontinentalen Innerasien (~30 kyr). Des Weiteren konnten mögliche Anzeichen für diagenetischbedingte Änderungen der Sedimentzusammensetzung und das Vorkommen von Karbonaten in der Sedimentabfolge des El´gygytgyn-Sees mit Hilfe von FTIRS gefunden werden. Die Resultate dieser Studie bekräftigen das große Potential der Fourier-Transformation-Infrarotspektroskopie in der Paläoklimaforschung.

Acknowledgements

First, I would like to thank my supervisor, Dr. Peter Rosén, for introducing me to the field of FTIRS, valuable comments, great support and guidance during this work. I would like to thank Prof. Dr. Martin Melles for giving me the opportunity to participate in the El´gygytgyn field campaign in 2009 and to complete my thesis under his supervision. Thank you for your support.

Particular thanks and gratitude go to Dr. Volker Wennrich and Dr. Hendrik Vogel for fruitful discussions, helpful advice, ideas, and great support. Furthermore, I am thankful to Prof. Dr. Per Persson for providing access to FTIRS laboratory at the Umeå University. I thank Bernhard Chapligin (Alfred Wegener Institute, Potsdam) for providing diatom samples, Dr. Stefan Krüger and Sylvia Dorn for performing XRD measurements at the University of Leipzig, and Nicole Mantke for support in the laboratory. Annette Hahn is thanked for checking the English spelling in this thesis.

Lastly, I particularly thank my parents who unremittingly supported me during my years of study and made this work possible.

Table of Contents

ANNEX

List of Figures

List of Tables

1 Introduction

The understanding of past environmental changes is of particular importance to facilitate the prediction of the magnitude and the regional repercussions of future environmental changes, especially in view of global-warming. Future changes are expected to be especially pronounced in the arctic regions which by now are experiencing environmental warming and change at rates unprecedented in historical times (OVERPECK et al. 2005; GREBMEIER et al. 2006). The Arctic plays a major role in the global climate system by triggering complex feedback processes involving the ocean, the atmosphere, the cryosphere and the continents. It is necessary to understand the function of the Arctic in the past in order to accurately predict future environmental changes. Therefore, long high resolution paleoclimate archives covering several glacial/interglacial cycles are required. Marine records of these time spans are available from the Arctic and sub-Arctic oceans (KEIGWIN 1998; THIEDE et al. 1998; NOWACZYK et al. (2001) in MELLES et al. 2007). In contrast, the longest terrestrial record of the Arctic from the Greenland ice sheet only extends back to the last interglacial period (NORTH GREENLAND ICE CORE PROJECT MEMBERS 2004). Hence, long continuous terrestrial records with a high temporal resolution are missing for comparison with marine records.

Lake El´gygytgyn situated in a 3.6 Ma old meteorite impact crater (LAYER 2000) in north-eastern Siberia contains such a terrestrial paleoclimate record. The region was most likely never covered by Quaternary ice sheets (GLUSHKOVA and SMIRNOV 2007) which enabled the formation of a continuous record that is probably the longest in the circumarctic (BRIGHAM-GRETTE et al. 2007). Two sedimentary records, PG1351 (~13 m long) and Lz1024 (16.60 m long), covering the last 250 (NOWACZYK et al. 2007) and 340 ka (MELLES et al. 2009), respectively, have been recovered from the lake during field campaigns in 1998 and 2003. In order to assess climatic and environmental changes in the Siberian Arctic, these records have been analyzed with regard to their paleo- and rock magnetic properties (NOWACZYK et al. 2002, 2007), their organic and inorganic geochemistry (MELLES et al 2007; MINYUK et al. 2007), their diatom and pollen records (CHERAPANOVA et al. 2007; LOZHKIN et al. 2007), and their clay mineralogy and sedimentology (ASIKAINEN et al. 2007). In winter 2008/2009, an ICDP (International Continental Scientific Drilling Program) funded deep drilling campaign was conducted at Lake El´gygytgyn. Besides a 142 m long permafrost core (D3), the entire sediment sequence of the lake of about 315 m (D1) was recovered. Since several analytical methods are required for the investigation of the sediment archive, the analysis of this long record is both time consuming and expensive.

Fourier transform infrared spectroscopy (FTIRS) is a promising tool for the rapid, simultaneous and therefore cost-efficient measurement of several proxies in sediment. Furthermore, the small amount of sample required for the measurement (0.01 g) facilitates an analysis in high resolution. FTIRS can be used for the determination of organic as well as minerogenic compounds. It has been applied to sediment to assess the concentration of silicate minerals (SIFEDDINE et al 1994; BERTAUX et al. 1996, 1998; WIRRMANN et al. 2001), and carbonates (MECOZZI et al. 2001), as well as to characterize humic substances (BRAGUGLIA et al. 1995; BELZILE et al. 1997; CALACE et al. 1999, 2006; MECOZZI and PIETRANTONIO 2006). FTIRS has also been used for the determination of tree-line changes and TOC in lake water (ROSÉN and PERSSON 2006). VOGEL et al. (2008) demonstrated that FTIRS can be used for the quantitative assessment of TOC, TN and BSi in the sediment record of core PG1351 from Lake El´gygytgyn by using an internal calibration set. Furthermore, ROSÉN et al. (2010) showed that reliable results for the BSi concentration in the sediments of core Lz1024 can be obtained by applying a FTIRS model based on sediment samples from Swedish lakes. However, this method has not been applied to sediment sequences that are very long in time and length like the entire sediment record of Lake El´gygytgyn (up to 3.6 Ma old and about 315 m long).

Aims of the Thesis:

(1) Development of robust FTIRS calibration models for the quantitative assessment of total carbon (TC), total organic carbon (TOC), total inorganic carbon (TIC), total nitrogen (TN), and biogenic silica (BSi) in the entire sediment record of Lake El´gygytgyn

(2) Comparison between resulting calibration models and already existing models based on the uppermost part of the sediment sequence (core Lz1024) (H. VOGEL, unpublished data)

(3) Application of the developed calibration models to sediments of marine isotope stage 11 (MIS 11) in high resolution to reconstruct past environmental and climatic changes

2 Study Area

This chapter provides a general description of Lake El´gygytgyn and the El´gygytgyn impact crater derived from previous studies. The geographical situation (see Section 2.1), the geological constitution (see Section 2.2) and the lake hydrology (see Section 2.3) are highlighted in this context.

2.1 Geographical Overview

Lake El´gygytgyn (67°30´ N, 172°05´ E) is located within the Anadyr Mountain Range in central Chukotka, north-eastern Siberia (see Figure 2.1). The lake is situated about 100 km north of the Arctic Circle and about 160 km southeast of the Chaun Bay, a bay of the Arctic Ocean.

Topography

The approximately circular shaped depression of Lake El´gygytgyn was formed by a meteoritic impact 3.6 Ma ago (LAYER 2000). The resulting crater has a diameter of roughly 18 km and the somewhat square shaped lake itself with a diameter of ca. 12 km is found in the southeastern part of the El´gygytgyn impact crater. The lake is situated at 492 m a.s.l. (above sea level) and the surrounding uplifted crater rim showing steep inner walls and gentle outer slopes extends from 600 m up to 935 m a.s.l. (MELLES et al. 2007). A watershed of 293 km^2 results from the specific crater morphology in which the water divide is practically defined by the crater rim. Furthermore, 110 km^2 of the watershed which is drained by about 50 ephemeral streams are covered by the lake surface itself (NOLAN and BRIGHAM-GRETTE 2007). Small, shallow gravel bar dammed lagoons occur at the lake shore, where the streams enter the lake. The Enmyvaam River represents the only outlet of Lake El´gygytgyn and drains the lake at its southeastern shore. The final receiving stream of the water from the lake is eventually the Anadyr River draining into the Bering Sea (BRIGHAM-GRETTE et al. 2007).

The lake bathymetry is characterized by shallow shelves (< 10 m deep) with steep slopes towards the broad flat bed of the lake basin (with slopes < 1°). The steepness of the slopes between the shelves and the deep basin ranges from 5-15° at the south and west shores and from 15-30° at the east and northeast shore. The maximum lake depth is 174 ± 2 m including 1 m of inter-annual lake level variation. The corresponding lake volume amounts to 14.1 km^3 (NOLAN and BRIGHAM-GRETTE 2007). According to GLUSKOVA (1993) in NOLAN and BRIGHAM-GRETTE (2007), Lake El´gygytgyn is located in a region of continuous permafrost with depths of 100-300 m and a maximum active layer depth of 0.8 m in the surrounding area of the lake in 2003 (SCHWAMMBORN et al. 2007). As a result of the heat capacity of water it is highly unlikely that permafrost is present beneath the lake (YERSHOV (1989) in MELLES et al. 2007).

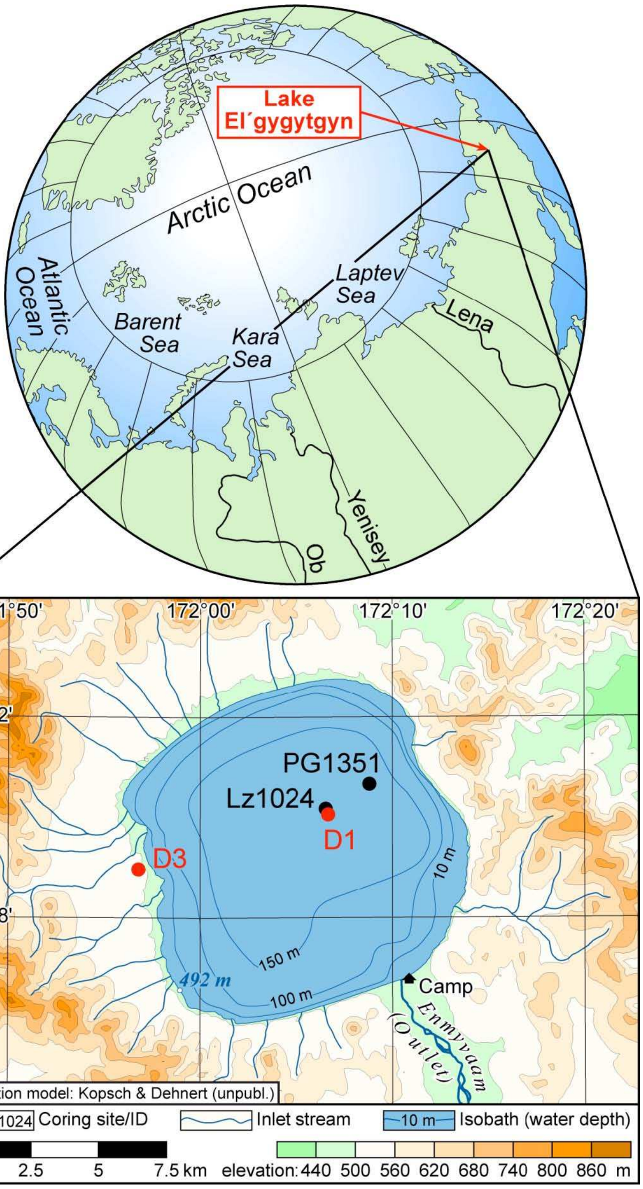

Figure 2.1 Maps showing the location of Lake El´gygytgyn in north-eastern Siberia (top) and the elevation model of the El´gygytgyn impact crater (bottom) illustrating the crater rim, the lake bathymetry and the locations of the recovered sediments (drill sites from 1998, 2003 (black) and winter 2008/2009 (red)) (after JUSCHUS et al. 2007 in MELLES in prep.).

Geomorphology

Large alluvial fans up to 3 km wide and 580 m a.s.l. high exist along the western and northern shore line of Lake El´gygytgyn. The southern and eastern shore is in contrast characterized by either narrow alluvial fans (< 0.5 km wide) or steep cliffs (up to 15 m high) (DEHNERT 2004). Geomorphological surveys and bathymetric soundings have distinguished four ancient lake terraces in the vicinity of Lake El´gygytgyn. These terraces are situated at 35-40 m (age: unknown), 9-11 m (age: begin of MIS 2) and 3-5 m above the recent lake level (minimum age: 13.2-14.2 ka BP). The fourth terrace is located 11-12 m below the recent lake surface (age: end of MIS 2) (BRIGHAM-GRETTE et al. 2005, JUSCHUS et al. subm.).

Several geomorphological surveys have shown that the region has never been affected by quaternary ice sheets and the nearest evidence for glacier activity was found 40 km to the west of the lake (GLUSHKOVA and SMIRNOV 2007).

Local Weather

In 2002, the MAAT (mean annual air temperature) at Lake El´gygytgyn was -10.3°C with a range from -40°C in winter to 26°C in summer. The annual precipitation amounted to ca. 180 mm in 2002 with 70 mm of summer rainfall and 110 mm snow water equivalent. Prevailing wind directions are either from the north or south with a mean hourly wind speed of 5.6 ms^{-1} in 2002. In 2002, the wind speeds exceed 13.4 ms^{-1} at least every month and 17.8 ms^{-1} in six of the months. Furthermore, the increased occurrence of strong winds is typical for winter months at Lake El´gygytgyn (NOLAN and BRIGHAM-GRETTE 2007).

Due to the extreme climate the open water season of Lake El´gygytgyn lasts for maximum three month of the year. The lake ice formation starts in late-October and attains a maximum ice thickness of 1.5-2.0 m. After the beginning of the snow melt in mid-May the disintegration of the lake ice begins with formation of a moat around the lake in mid-June. Ice freeness is reached around the middle of July.

Vegetation

The modern vegetation in the basin of Lake El´gygytgyn is dominated by lichen and herb species with a mainly discontinuous occurrence. Local patches of low-growth shrub forms like willows (*Salix spp.*) and dwarf birches (*Betula nana*) are found in protected areas like mountain valleys and in areas with a high organic accumulation. The surrounding Chukchi upland is characterized by tundra with low-shrub and herb domination. The modern tree line with light coniferous forests is found about 150 km to the south and west of Lake El´gygytgyn (LOZHKIN et al. 2007).

2.2 Geological Overview

The Lake El´gygytgyn impact crater is situated in the Okhotsk-Chukotka volcanic belt (OCVB), one of the largest subduction related volcanic provinces of the world. The cretaceous OCVB originated from Andean-style volcanism due to subduction of the Kula oceanic plate under the Verkhoyansk-Chukotka orogen. It extends for ca. 3200 km and comprises approximately 1.2 million km^3 of volcanic and associated plutonic rocks. Further, the extrusive rocks overlie the Verkhoyanks-Chukotka structures with an angular unconformity and are undeformed (ISPOLATOV et al. 2004). Their rock composition varies from mafic (basalt) to felsic (rhyolite) and broad areas are covered with tuffs and large ignimbrites (KELLEY et al. 1999).

According to NOWACZYK et al. (2002), it is possible to subdivide the rocks in the vicinity of Lake El´gygytgyn into four geological units (see Figure 2.2). The first unit, the Pykavaam Formation, captures the main part of the area and encloses the lake with the exception of the southeastern lake surroundings. The formation with a strongly variable thickness of 50-1,000 m consists of rhyolitic ignimbrites and tuffs (KELLEY et al. 1999). The occurrence of the second unit, the Voron´ina Formation, is limited to the crater rim to the east. This formation is characterized by ignimbrites of dacite and andesite-dacite composition, acid to moderately-acid tuffs and tuffaceous clastic rocks. Their thicknesses differ from 50 to 550 m (KELLEY et al. 1999). Outcrops of the third unit, the Koekvun Formation, are found to the southeast of Lake El´gygytgyn on both sides of the Enmyvaam River as well as to the east of the lake. This formation consists of basalts, andesite-basalts and different types of vulcaniclastic deposits (tuff-breccia, sandstone, and tuff-siltstone) (Nowaczyk et al. 2002). The Koekvun Formation reaches a maximum thickness of up to 550 m (KELLEY et al 1999). The fourth formation, the Ergyvam Formation, occurs alongside the eastern crater rim as well as at a few outcrops to the south of the lake. This formation consists of ignimbrites and tuffs with rhyolitic composition and has a maximum thickness of 300 m (BELYI et al. 1997 in DEHNERT

2004). The Pykavaam Formation, the Voron´ina Formation and the Koekvun Formation are part of the Chauna Group that is located in the northern part of the OCVB. New ^{40}Ar/^{39}Ar dates show an age for the beginning of the volcanism in this area of ca. 88 Ma (Coniacian (Upper Cretaceous)) and a short duration of activity (ca. 1-6 Myr) (Kelley et al. 1999; Isopalatov et al. 2004).

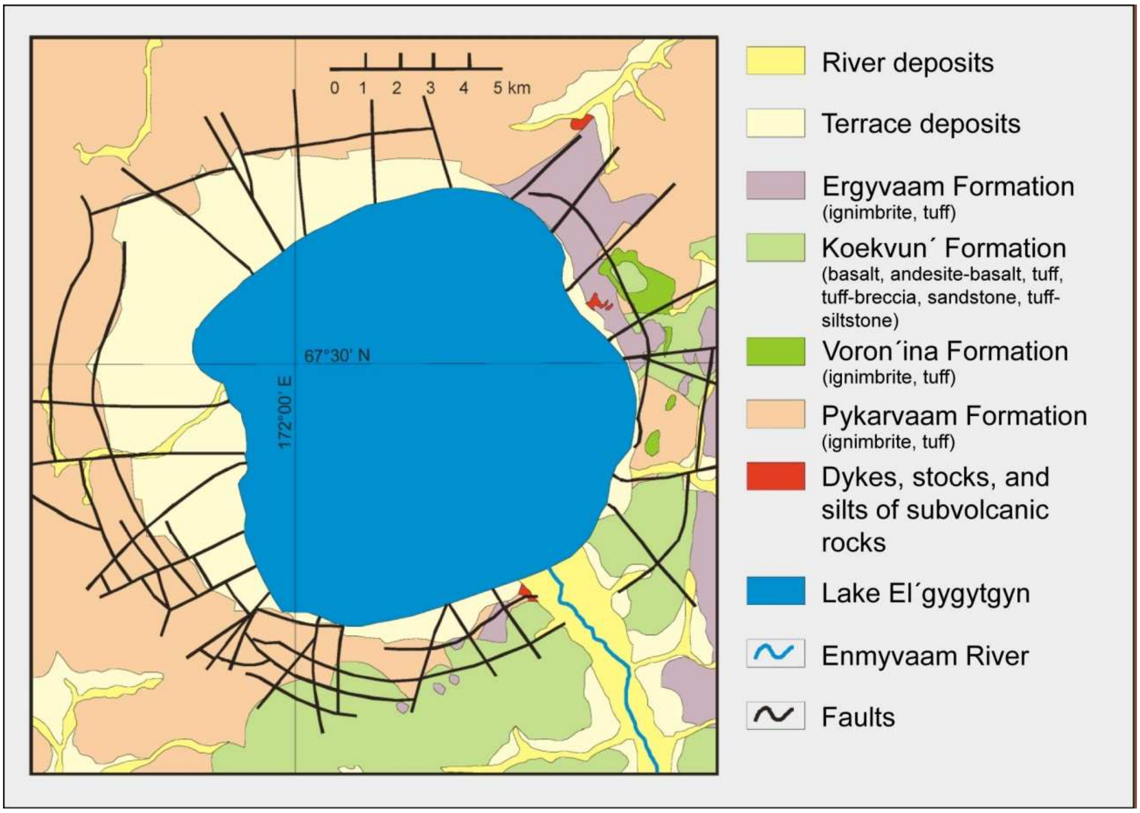

Figure 2.2 Schematic geological map of the El´gygytgyn impact crater (from Dehnert 2004: geology after Nowaczyk et al. 2000; fault system after Belyi and Chereshnev (1993) in Dehnert 2004).

The meteorite impact has an ^{40}Ar/^{39}Ar age of 3.58 ± 0.04 Ma (Layer 2000) and created a complex system of faults around the Lake El´gygytgyn impact crater. This system is predominated by short radial faults, with subordinated concentric arcuate faults. The length of the faults varies from 0.5 to 10 km and the highest fault density is found at the inner walls of the impact structure (Gurov and Koeberl 2004). Seismic surveys have shown a central uplift morphology in the form of a concentric inner ring which is covered by brecciated material and lake sediments (Gebhardt et al. 2005).

2.3 Lake Hydrology

Lake El´gygytgyn is a cold-monomictic and ultra-oligotrophic lake with slightly acidic pH (6.3-6.6) (CREMER and WAGNER 2003; MELLES et al. 2007). Temperature profiles recorded from summer 2000 to summer 2003 show that the water column of the lake is thermally stratified during winter and that the water temperature of the entire water body never exceeds 4°C. Complete mixing of the water column and consequently isothermal conditions occur during summer (NOLAN and BRIGHAM-GRETTE 2007). The breakup of stratification is supported by vertical profiles of temperature, conductivity, pH, oxygen saturation, and cation and anion concentrations with only minor variations in the summer of 2000 (CREMER and WAGNER 2003).

Increasing values of conductivity and pH close to the lake floor indicate some exchange between the lake water and the sediments (MELLES et al. 2007). The distinct decrease of oxygen saturation to ca. 95% below 150 m water depth points to an intensified oxic decomposition of organic matter and a reduced mixing in the lowermost part of the water column (CREMER and WAGNER 2003). The low suspension load in Lake El´gygytgyn is reflected by very clear surface water and a Secchi depth of 19 m in the summer of 2000.

3 Material and Methods

The following chapter gives an overview about the methodological approach with brief explanations of the methods used in this study (see Figure 3.1). Sample origin, conventional measurements and FTIR measurements including an introduction into the theoretical background of this method are described under field and laboratory methods (see Section 3.1). Furthermore, the steps of the model development between FTIRS derived spectral information and conventionally measured reference data are shown in Section 3.2.

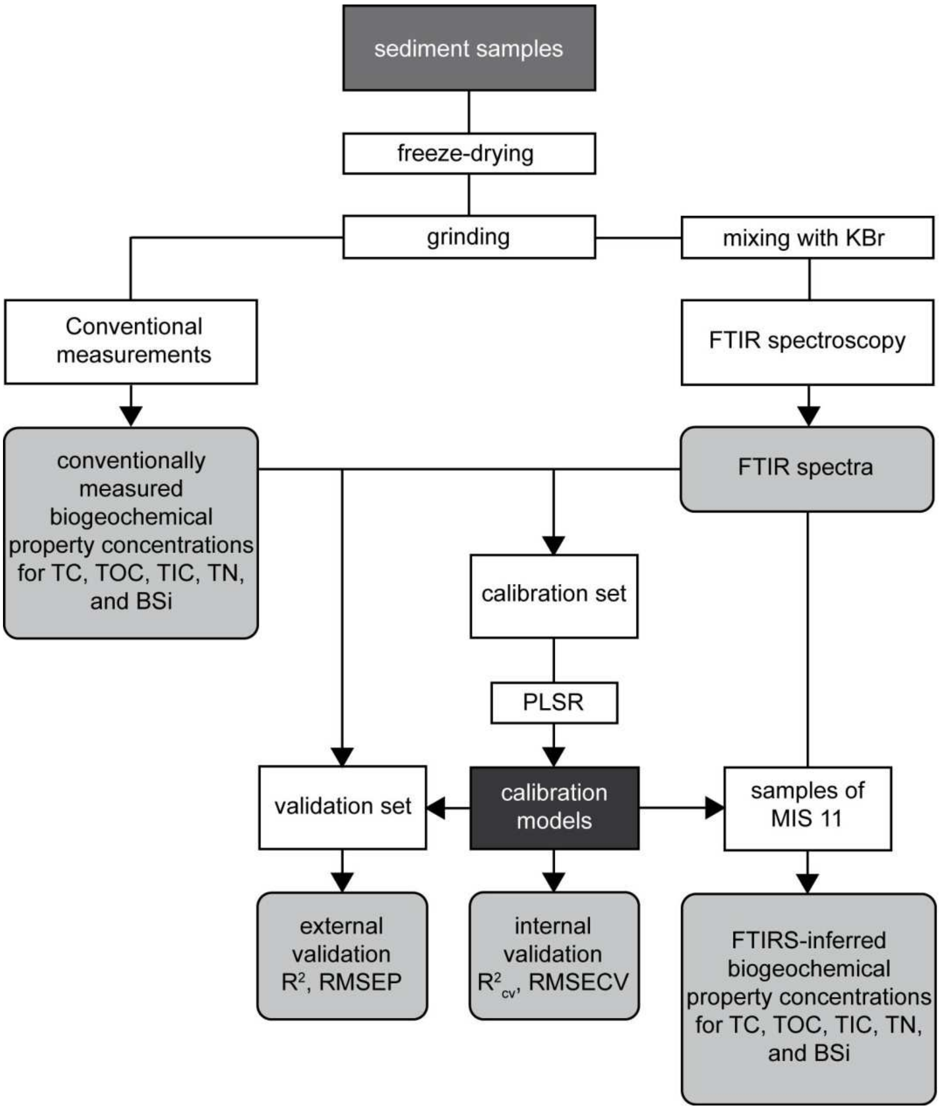

Figure 3.1 Flow chart of the methodological approach for the quantitative estimation of biogeochemical properties in sediment by means of Fourier transform infrared spectroscopy (FTIRS) and Partial Least Squares Regression (PLSR).

3.1 Field and Laboratory Methods

3.1.1 Samples

The sediment samples used for model development and model-application to MIS 11 were taken from cores recovered during the El´gygytgyn Drilling Project field campaign in January to May 2009. The on ice drilling operations were performed by DOSECC (Drilling, Observation and Sampling of the Earth´s Continental Crust Inc., USA) using a GLAD-800 drilling system (Global Lake Drilling 800 m). During the operation, different coring tools depending on the sediment characteristics of the drilled section were used for core recovery. Tools like the Hydraulic Piston Corer (HPC), the non-rotating Extended Shoe (Extended Nose (EXT)) and the rotating Extended Core Bit (Alien (ALN)) were applied. The lake sediments were sampled down to the underlying impact breccia at 315 mblf (meters below lake floor) at location D1 (see Figure 2.1) which is situated in the deepest part of Lake El´gygytgyn (ca. 175 mblf). Due to the fact that the sediment record of D1 was recovered in three holes (1A, 1B and 1C) a composite profile was established. 349 samples of the composite profile were available for the model development yielding an average resolution of ca. 1 m and a maximum distance between two samples of < 3 m for D1. The sampling of the composite profile occurred on-site at each cut surface after cutting the 3 m long cores into 1 m sections. In addition, 31 samples arising from the core section related to MIS 11 itself were also used for the model development and were taken along with the samples for the model-application in the laboratory in December 2009. The 1.69 m long core section related to MIS 11 (14.97-16.66 mblf) was subsampled in 2.5 mm intervals yielding 677 samples. The position of the deposits of MIS 11 in the sediment record of D1 was determined with the help of previous results from the cores PG1351 (1998) and Lz1024 (2003). The lithostratigraphy (MELLES et al. 2007) and the known location of younger isotope stages were helpful in this context.

FTIR calibration models used for the comparison with calibration models resulting from this study are based on sediments from core Lz1024, which was recovered through holes in the lake ice cover during an expedition in 2003. The composite core covers the uppermost 16.60 m of the sediment record of Lake El´gygytgyn and was obtained by using a gravity corer (UWITEC Ltd., Austria) for the uppermost sediment decimeters and a percussion piston corer (UWITEC Ltd., Austria) for the deeper sediments (JUSCHUS et al. 2005). Core Lz1024 was subsampled in 1 cm intervals.

For comparative purposes, samples of porcelanite, tephra, and diatom assemblages were analyzed by FTIR spectroscopy as well. The porcelanite samples with a high degree of purity were collected in Morocco (Jbel Tilda, Meskala Formation, Lutetian (40.4-48.6 Ma)) (H.-G. HERBIG, pers. commun. 2010), while the tephra sample (D1; field depth: 5.15 mblf) and the diatom samples (Lz1024) arise from Lake El´gygytgyn itself. Clean diatom samples with a degree of purity > 96% have been gained after various preparation steps including H_2O_2/HCl treatment, sieving and heavy liquid separation. The preparation of the diatom samples was effected at the Alfred Wegener Institute (Potsdam, Germany).

3.1.2 Conventional Measurement of Biogeochemistry

The conventionally measured biogeochemical property concentrations were used as reference data (primary data) for the development of calibration models. All sediment samples were freeze-dried with a beta 1-8 LD plus freeze dryer (Martin Christ Corp.) and ground to a particle size < 63 µm using a MM2 swing mill (Retsch Corp.). Measurements of total carbon (TC) and total nitrogen (TN) were conducted with a vario MICRO cube element analyzer (Elementar Corp.). The element analyzer combusts the sample material stored in sealed tin vessel at 1,150°C and successively determines the element concentrations using a thermal conductivity detector. TC and total inorganic carbon (TIC) were also determined per suspension method using a DIMATOC® 100 liquid analyzer (Dimatec Corp.). In this method, the sample material is mixed with distilled water and remains in suspension during the entire measurement. Both parameters are analyzed simultaneous in two independent channels and detected by absorption of infrared radiation from the released CO_2. The CO_2 release from inorganic carbon is based on the reaction between carbonate ($CaCO_3$) and 40 percent phosphoric acid (H_3PO_4) at 160°C, while the CO_2 release from total carbon is caused by the combustion of the sample material at 890°C. The advantage of liquid analysis compared to the combustion method of the element analyzer is that one sample can be measured several times. The setup used for the samples of this study included three repetitions per sample. To facilitate the differentiation between the two results obtained for TC, data derived from vario MICRO cube element analyzer are abbreviated as $TC_{(EA)}$ and data resulting from DIMATOC® 100 liquid analyzer are abbreviated as $TC_{(LA)}$. Total organic carbon (TOC) was calculated by subtracting TIC from $TC_{(LA)}$.

Concentrations of biogenic silica (BSi, Opal) were analyzed by applying the wet chemical leaching method according to MÜLLER and SCHNEIDER (1993). In this method, the opaline material is extracted by 1 M NaOH at 85°C, and the resulting increase in dissolved silica is continuously monitored. The detection of dissolved silicon is effected by molybdate-blue spectrophotometry. The resulting plot of absorbance versus time is then evaluated according to the extrapolation procedure of DEMASTER (1981).

The conventional measurements of TC, TN and BSi used for the establishment of calibration models for core Lz1024 are based on the same methods used in this study. TC and TN were measured with a CHNS-932 analyzer (LECO Corp.) and BSi measurements were conducted according to the wet chemical method described by MÜLLER and SCHNEIDER (1993). In core Lz1024, TOC and TIC were determined with a different method than the one used in this study. The samples for the TOC measurement were pretreated with 10 percent hydrochloric acid (HCL) at a temperature of 80°C to remove the contained carbonate and then analyzed by using a Metalyt-CS-1000-S (ELTRA Corp.). TIC was determined by subtracting TOC from TC.

X-ray diffraction (XRD) measurements were performed at the University of Leipzig (Germany) to identify the kind of carbonate mineral contained in the sediment record of Lake El´gygytgyn. 1 g of ground sediment mixed with an internal standard of corundum (α-Al_2O_3,) at a sample/standard ratio of 5:1 was analyzed by using a MiniFlex X-ray diffractometer (CoKα anode, 30 kV, 15 mA, 1.7903 Å) (Rigaku Corp.). The samples were X-rayed in the region from 3-40° 2Θ with a step size of 0.02° 2Θ and a measuring time of 2 s per step. The evaluation of the diffractograms was effected as described in NEUMANN and EHRMANN (2001).

3.1.3 Fourier Transform Infrared Spectroscopy (FTIRS)

Theoretical Background

Infrared radiation (IR) is among the electromagnetic waves or electromagnetic radiation which consists of electric and magnetic fields oscillating in phase, perpendicular to each other and perpendicular to the direction of energy propagation (HARRIS 2007). Electromagnetic radiation is characterized by its wavelength $\boldsymbol{\lambda}$ (crest-to-crest distance between waves) and its frequency $\boldsymbol{v}$ (number of complete oscillations of a wave per second). The unit of wavelength is cm and the unit of frequency s^{-1}. One oscillation per second is also called one hertz (Hz). In addition to wavelength, the unit wavenumber $\bar{\boldsymbol{v}}$ is common in the literature for the description of IR spectra. The wavenumber expressed in cm^{-1} is the number of waves in a 1 cm long wave train and is related to the wavelength and frequency according to Equation 3.1 and Equation 3.2:

$$\bar{v} = \frac{v}{c} \qquad \text{(Equation 3.1)}$$

and

$$\bar{v} = \frac{1}{\lambda} \qquad \text{(Equation 3.2)}$$

where $\boldsymbol{c}$ is the velocity of light, 2.997925×10^{10} cm/sec. The IR part of the electromagnetic spectrum covers the wavelength range from 7.8×10^{-5} to 1×10^{-1} cm, or the wavenumber range from 12,800 to 10 cm^{-1}. Further, infrared radiation is subdivided into near infrared (7.8×10^{-5} to 2.5 × 10-4 cm or 12,800 to 4,000 cm^{-1}), mid infrared (2.5×10^{-4} to 5×10^{-3} cm or 4,000 to 200 cm^{-1}) and far infrared (5×10^{-3} to 1×10^{-1} cm or 200 to 10 cm^{-1}) (COLTHUP et al. 1975). The used wavelength section in Fourier transform infrared spectroscopy is the mid infrared region.

The basic principle of the IR spectroscopy is the excitation of polar bonds of molecules by absorption of light in the infrared region of the electromagnetic spectrum. Absorption is primarily between atoms of hydrogen, carbon, oxygen and nitrogen, the so called light atomic bonds (e.g. C-H, C-O, C=C). It causes molecular vibrations with a life time in the order of 10^{-9} - 10^{-6} s after excitation. The frequency or wavelength at which atoms of a molecule are excited and start to vibrate is dependent on the types of vibrating atoms (atomic mass and radius), the bond strength and the structure of the molecules. These mass and structural dependent vibrations are called normal vibrations. Normal vibrations are developed as discrete vibrations of all atoms of a molecule moving in phase with the same frequency but with different amplitudes (KELLNER et al. 2004, HARRIS 2007). The fundamental modes of normal vibrations are stretching (stretching and shortening of chemical bonds, symmetric or asymmetric), bending (in-plane movement of atoms changing the angle between bonds), wagging (in-phase, out-of-plane movement of atoms, while other atoms of the molecule are in-plane), rocking (in-phase forth and back swinging of atoms in the symmetry plane of the molecule), and twisting (rocking vibration with twisting of the plane during the movement of the atoms) (TWARDOWSKI and ANZENBACHER 1994). The high sensitivity to changes in composition and structure of normal vibration facilitates a fingerprint-type identification of polyatomic molecules. IR radiation only causes vibration in polar bonds in which a change of the dipole moment occurs. Due to this fact, non-polar molecules cannot be identified by IR spectroscopy (KELLNER et al. 2004).

Compared to normal vibrations, absorption bands of functional groups are independent of structure and composition of the molecules. This independence occurs if the atoms constituting the functional group are significantly lighter or heavier than the neighbouring atoms or if the bond strength in the functional groups differs from those of the bonds in the vicinity. The absorption of functional groups is called group frequency and significantly developed by functional groups containing H atoms or isolated double and triple bonds. The corresponding wavelength region of group frequencies is situated at wavenumber positions higher than 1300 cm^{-1} and groups containing heavy atoms are found in the FIR region below 400 cm^{-1}. The wavelength range from 1,300 to 400 cm^{-1} is called the fingerprint region and contains bands of absorbance of special significance for the entire molecule (KELLNER et al. 2004). With regard to the aim of this thesis; the analysis of sediments, IR spectroscopy enables the identification of both organic and minerogenic components, whereas spectral regions related to minerogenic components are mostly situated in the fingerprint region due to the missing of functional groups with the exception of hydroxyl group.

The basis for quantitative analysis of certain sediment components is the Bouger-Lambert-Beer law (see Equation 3.3) which demonstrates the direct proportionality of absorbance $\boldsymbol{A}$ to concentration, $\boldsymbol{C}$, of the light-absorbing species in the sample. The absorbance is expressed as

$$A = \varepsilon b C \qquad \text{(Equation 3.3)}$$

where $\boldsymbol{\varepsilon}$ is the molar absorptivity (M^{-1} cm^{-1}) and $\boldsymbol{b}$ is the pathlength (cm). Absorbance is dimensionless, but the term “absorbance units” after absorbance can be found in the literature. The concentration is usually given in units of moles per liter (M) (HARRIS 2007). A correct estimation of concentration of a single compound by integrating of peak areas is difficult due to overlapping of various absorbance bands, especially within mixtures like sediments that contain many different compounds. Other common methods based on the peak height, the maximum absorbance, at a certain frequency are affected by the additive character of absorbance. Therefore the integration of multivariate techniques has been a major advance in quantitative analysis of IR spectra and is now commonly used for data extraction (see Section 3.2) (GRIFFITHS and DE HASETH 2007).

The sampling technique used for IR analysis depends on various sample properties like the aggregate state, the crystallinity or the IR region of interest. The powdered, solid sediment samples of this study were analyzed by means of the diffuse reflectance technique which is a simple way to measure samples without a smooth, cleanly reflecting surface (JOHNSTON 1991). Diffuse reflection results from the scattering by a combination of reflection, refraction and diffraction when incident radiation strikes the rough surface of a powdered sample. The reemerged radiation is then called diffusely reflected. The relationship between reflectance $\boldsymbol{R}$ and absorbance $\boldsymbol{A}$ is expressed according to Equation 3.4:

$$A = \log\left(\frac{1}{R}\right) \qquad \text{(Equation 3.4)}$$

One of the major sources of interference is specular or Fresnel reflection resulting from the direct reflection at the front surface of a particle which is measured along with the diffuse reflected radiation. Therefore, the sample material is diluted with non-absorbing alkali halides like KBr or KCl to minimize the influence of specular radiation on the IR-spectra (GRIFFITHS and DE HASETH 2007). Furthermore, a high ratio between diluent and sample avoids very high absorbance (> 3.0) causing low intensities of IR radiation reaching the detector. This can produce noisy data due to a low signal-to-noise ratio (HERBERT et al. 1992). However, several studies have shown that significant results can be obtained without sample dilution (REEVES et al. 2001; REEVES 2003; SIEBIELEC et al. 2004).

Fourier transform infrared (FTIR) spectrometer basically consists of a light source, an interferometer, and a detector. Silicon carbide rods, so called “globars”, electrically heated to approximately 1100°C are the most frequently used sources for MIR spectroscopy and the most common IR detectors are pyroelectric deuterated triglycine sulphate (DTGS) and photoconducting mercury cadmium telluride (MCT) detectors. The interferometer which allows the simultaneous measurement of all wavelengths in the MIR range essentially consists of a beamsplitter, a fixed mirror, a movable mirror, and a drive and positioning mechanism. The radiation of the source is equally divided by the beamsplitter and directed to the fixed and the movable mirror. The moving mirror is scanned at constant velocity resulting in changing optical path differences of the two beams as a function of time. The reflected beams interfere at the beamsplitter, from where 50% of the radiation returns to the source, and 50% reaches the detector. The intensity of the radiation at the detector is a function of the optical path difference of the beams in both arms of the interferometer. The resulting interferogram then requires the mathematical Fourier transformation to obtain the desired IR spectrum (KELLNER et al. 2004). Due to the absorption of IR radiation by the sample placed between the interferometer and the detector, the recorded interferogram contains the emitted spectrum of the source minus the absorption spectrum of the sample. The FTIR technique requires the recording of a background spectrum prior to the actual sample analysis. This spectrum based on the measurement of pure diluting substance is then subtracted from the spectrum of sample material diluted in the non-absorbing diluent (KELLNER et al. 2004; GRIFFITHS and DE HASETH 2007; HARRIS 2007).

FTIR-Measurement

The IR spectral information used for the model development were recorded by FTIR spectroscopy. Previous to the FTIR measurement, all samples were freeze-dried (beta 1-8 LD plus freeze dryer (Martin Christ Corp.) and ground to a particle size < 63 µm (MM2 swing mill (Retsch Corp.)). 0.011 g sample material was then mixed with 0.5 g spectroscopic grade potassium bromide (KBr) (Uvasol®, Merck Corp.), which does not influence the FTIR spectrum due to its transparency in the IR region. The sample was homogenized using a mortar and pestle. The hygroscopic KBr was dried in an oven at 450°C to minimize the effect of not chemically combined water on the spectra. The low sample concentration (~ 2.2%) was chosen to avoid spectral distortions by very high absorbance and optical effects. To gain constant measuring conditions and avoid variability caused by variations of temperature, the measurement was performed in a temperature controlled laboratory with a constant temperature of 25 ± 0.2°C. Samples were stored in the temperature controlled room at least 5 h prior to the measurement. The prepared samples were placed in a sample cup and analyzed by means of the diffuse reflectance FTIRS technique. A Bruker IFS 66v/S FTIR spectrometer (Bruker Optics Inc.) equipped with a diffuse reflectance accessory (Harrick Inc.) was used for the analysis under vacuum (4 mbar). The used setup of 64 repeat scans per sample in ~2 cm^{-1} resolution for the wavelength range from 2,666 to 25,000 nm, or from 3,750 to 400 cm^{-1} yields 1737 data points per sample. In this study, FTIRS was applied to a set of 380 samples used for the model development and to a set of 677 samples from MIS 11 to which the developed models were applied.

3.2 Model Development

The major problem of IR spectroscopy is the handling of the large number of data (1737 data points per sample) which is intensified by the overlapping of spectral information, especially in sediment samples consisting of various compounds (see Section 3.1). The extraction of qualitative and particularly of quantitative information about organic and minerogenic compounds solely by visual analysis is extremely difficult. In this context, multivariate techniques are commonly used tools to relate the complex spectral information to the reference data of interest (biogeochemical property concentrations). In addition to multivariate regression methods used for the construction of calibration models, data processing of the IR spectra is required.

Baseline Correction and Multiplicative Scatter Correction (MSC)

Prior to the model development, baseline correction and multiplicative scatter correction were applied to normalize the recorded FTIR spectra enabling an improved intercomparison of all measured samples. The baseline correction compensates baseline shifts and tilting caused by internal variations of the FTIR spectrometer during the measurement. This method generates the same baseline for all FTIR spectra by means of linear correction setting two points or regions which contain no spectral information to zero. In this study, the spectral region between 2,210 and 2,200, as well as absorption at around 3,750 cm^{-1} were set to zero.

Multiplicative scatter correction is used to remove spectral variations (noise) resulting from sample inhomogeneities and optical effects. The basic principle of MSC is that an approximately straight line results from plotting the reflectance values of a sample against the reflectance values of the mean of all samples for each wavelength. The intercept and slope of the resulting line are estimated for each sample by means of linear regression. Each spectrum can then be corrected using these estimations. The remaining spectral variations are supposed to be related solely to the specific molecular vibrations depending on the chemical composition of the sample and free from scattering effects. The intercept (additional effect) is primarily caused by specular reflectance, while the slope (multiplicative effect) is due to sample inhomogeneities like grain-size variations (GELADI et al. 1985; MARTENS and NÆS 1989; ANDRADE et al. 1997).

Principle Component Analysis (PCA) and Partial Least Squares Regression (PLSR)

Partial least squares regression was used to develop calibration models between FTIR spectral information and the corresponding conventionally measured biogeochemical properties. PLSR as well as Principle Component Analysis are based on the simplification of a large number of variables to a few underlying variables describing the main variation in the data. PCA uses a $\boldsymbol{N} \times \boldsymbol{K}$ data matrix (**X**) consisting of **N** samples and **K** variables which are in this case the corresponding absorbance values of each sample at each wavelength. In this matrix, each sample (**N**) can be described as a point in the **K** dimensional variable space resulting from plotting all **K** variables against each other. By applying PCA, a set of principle components (PCs) which create a hyperplane with several dimensions are constructed in the variable space. This hyperplane explains as much spectral variations in the samples as possible. It can be extracted and viewed as a two dimensional plane or line plot. The first principle component (PC1) describes the largest spectral variation, the second principle component (PC2) perpendicular to PC1, the second largest variation and so on until **A** principle components are constructed. The resulting $\boldsymbol{N} \times \boldsymbol{A}$ matrix, the so called score matrix **T**, creates a new variable space consisting of dimensionless latent variables (scores) for each $PC_{(t1\text{-}ta)}$ within the **K** dimensional space and explains the changes in the sediment composition. The corresponding loading vectors establish a $\boldsymbol{K} \times \boldsymbol{A}$ matrix, the so called loading matrix **P**, which shows the influence of each wavelength (K) on the $PC_{(t1\text{-}ta)}$ (MARTENS and NÆS 1985, ANTTI 1999).

The main difference between PCA and PLSR is that in PLSR the target value **Y**, in this case, the concentration of certain sediment compounds, is actively used. PLSR establishes a relationship between the **X**-matrix and the **Y**-matrix by relating their scores in order to find the maximum of covariance between both datasets. This means that the variation in the FTIR spectra (absorbance at each wavelength per sample) is used to explain the variation in the biogeochemical properties. Since PLS analysis can be viewed as the regression extension of PCA, the variations in the **X**-matrix are described by the **X**-scores, **T**, for each PLS $\text{component}_{(t1\text{-}ta)}$ and the corresponding variation within the **Y**-matrix by the **Y**-scores, **U**. In PLS, the covariance between these latent variables, **T** and **U**, is maximized (MARTENS and NÆS 1985, ANTTI 1999). Calibration models for the prediction of biogeochemical property concentrations from FTIR spectra of new samples can then be constructed based on the linear relationship between the spectral information of the FTIR measurement and concentrations of conventionally measured biogeochemical properties. The corresponding loadings of each PLS component$_{(t1\text{-}ta)}$ of a model show the contribution of each wavelength of the component$_{(t1\text{-}ta)}$ to the calibration model and with it to the prediction of a certain biogeochemical property concentration. The loadings of the first PLS component explain the largest part of the spectral variation depending on the variation within the primary data. Therefore, they were used in this study to identify the spectral region contributing the most to the correlation.

Calibration models between FTIR spectral information and the conventionally measured biogeochemical properties were developed and then applied to samples from the core section related to MIS 11 to infer environmental and climatic changes during that period. Conventionally measured biogeochemical data were available for BSi (183 samples), TC$_{(EA)}$, TN (197 samples), and TC$_{(LA)}$, TIC and TOC (204 samples). The samples with known biogeochemical concentrations were split into two sets of samples, the calibration set and the validation set. 50 samples were used in the validation set to assess the prediction ability of the models (see below) and the remaining samples were used in the calibration set to establish the calibration models. All biogeochemical property concentrations available for the model development are listed in Table A.1 and A.2 in the annex. Outliers were identified by means of the conventionally measured vs. FTIR-inferred plot. If the outliers had a large influence on the calibration model they were removed from the calibration set to improve the statistical performance of the corresponding model. The occurrence of outliers can arise from the conventional measurements as well as from the FTIR measurements. Potential reasons for outlier are sample contamination, strong differences in the sample composition (e.g. grain-size effects), variability in the sample pretreatment or the measurement conditions. Calibration models derived from core Lz1024 (H. VOGEL, unpublished data) are based on 1,657 samples for TC, TOC, TN and on 201 samples for BSi.

Model Validation

In multivariate calibrations, quantitative assessments of model performance are used to estimate the complexity and the prediction ability of a calibration model. Both internal and external validations were applied in this study. The internal validation is based on samples already used in the calibration model, whereas the external validation is based on samples unknown for the model. The internal validation was performed by cross validation (CV) and evaluates how much of the variation in the primary data is predicted by the model. In particular it assesses the significance of each model component. By applying CV, the primary dataset, in this case, the conventionally measured concentrations of a biogeochemical property, is divided into a number of groups from which one group in turn is excluded. The biogeochemical property concentration of the samples in this group is then predicted solely based on the corresponding spectral information by a model build on the primary data within the remaining groups. This procedure is repeated until every group has been predicted. In this context, the cross validated coefficient of determination R^2_{cv} and the root mean square error of cross validation (RMSECV) (see Equation 3.5) were used to evaluate the internal model prediction. RMSECV was calculated by

$$\mathrm{RMSECV} = \frac{1}{n}\sqrt{\frac{\sum_{i=1}^{n}(y_i - \hat{y}_i)^2}{\sum_{i=1}^{n}(y_i - \bar{y})^2}} \qquad \text{(Equation 3.5)}$$

where n is the number of samples, y_i the conventionally measured concentration of a particular biogeochemical property, $\hat{y}_i$ the predicted property concentration and $\bar{y}$ the mean concentration of the conventionally measured property of all samples.

The external validation was performed on the 50 samples of the validation set covering the entire composite profile of D1. The coefficient of determination R_2 between conventionally measured and FTIR inferred biogeochemical property concentration, as well as the root mean square error of prediction (RMSEP) (see Equation 3.6) were used to estimate the prediction ability of developed calibration models solely depending on FTIR spectra. RMSEP was calculated by

$$\mathrm{RMSEP} = \sqrt{\frac{\sum_{i=1}^{n}(y_i - \hat{y}_i)^2}{n}} \qquad \text{(Equation 3.6)}$$

where n is the number of samples, y_i the conventionally measured biogeochemical concentration and $\hat{y}_i$ the predicted biogeochemical property concentration. The calibration models derived from core Lz1024 were also applied to the validation set to enable the comparison with the models developed in this study.

PCA was performed on the samples of the core section related to the MIS 11. This allowed an overview of the occurring spectral variations within the record independent of the conventionally measured biogeochemical data. The loadings of the first principle component were then used to estimate the contribution of each wavelength to the variations. All multivariate data analysis was conducted by SIMCA-P 10.0 (Umetrics AB, SE-907 19 Umeå, Sweden) and the software OPUS 5.5 (Bruker Optics Inc.) was used for the visualization of single FTIR spectra.

4 Results, Discussion and Interpretation

This chapter sets out the results of the study which are subsequently discussed and interpreted. First, the general information contained in the FTIR spectra are highlighted (see Section 4.1), followed by the analysis of the model development. The statistical performance and relation to the biogeochemistry are demonstrated for each FTIRS calibration model in this context (see Section 4.2). The resulting models of this study are then compared with already existing FTIRS models derived from core Lz1024 (H. VOGEL, unpublished data) (see Section 4.3).Furthermore, the models of this study are applied to sediments of Lake El´gygytgyn covering the MIS 11 to reconstruct climatic and environmental changes (see Section 4.4). Finally, potential diagenetic changes (see Section 4.5) and the occurrence of carbonates (see Section 4.6) in the sediment record are presented.

4.1 Spectral Information

The FTIR spectrum of a representative sample from the sediment record of Lake El´gygytgyn shows highest absorbance in the spectral region from 950-1,200 cm^{-1} with distinctive peaks at around 1,050 and 1,100 cm^{-1} (see Figure 4.1). This region can be ascribed to asymmetric Si-O-Si and Si-O-(Al) stretching vibrations of silicates (MOENKE 1974b). Previous studies of the sediment composition have shown that clay minerals like smectite, illite, chlorite (ASIKAINEN et al. 2007) and kaolinite, as well as feldspar, quartz (DEHNERT 2004) and opal (biogenic silica) (MELLES et al. 2007) are the major compounds of the sediment record of Lake El´gygytgyn. SiO molecular vibrations of these silicates can be related to the distinctive peaks at around 1,050 cm^{-1} (clay minerals, feldspars) and at around 1,100 cm^{-1} (Opal) (FARMER 1974; MOENKE 1974b; MADEJOVÁ 2003). The SiO molecular vibrations of quartz cannot be clearly assigned to one of both peaks. Absorption bands of organic compounds, e.g. caused by C-O-C and -C-O stretching vibrations of carbohydrates (MECOZZI and PIETRANTONIO 2006), can be attributed to the spectral region of highest absorption as well. Organic matter is only a minor component of the sediments from Lake El´gygytgyn (highest conventionally measured TOC content of this study: 2.9%, previous studies: 2.5%

(Melles et al. 2007)). Therefore, it is very likely that this part of the FTIR spectrum is related mostly to minerogenic compounds. The second strongest absorption band lies between 400 and 550 cm^{-1} and can be assigned to O-Si-O bending vibrations of silicates. Furthermore, absorbance of medium intensity between 550 and 850 cm^{-1} can also be ascribed to molecular vibrations in silicates and are the consequence of their polymerized structure (Moenke 1974b). Distinctive absorbance peaks in these regions can be found at 440, 470, 525, 595, 645, 695, and 800 cm^{-1}.

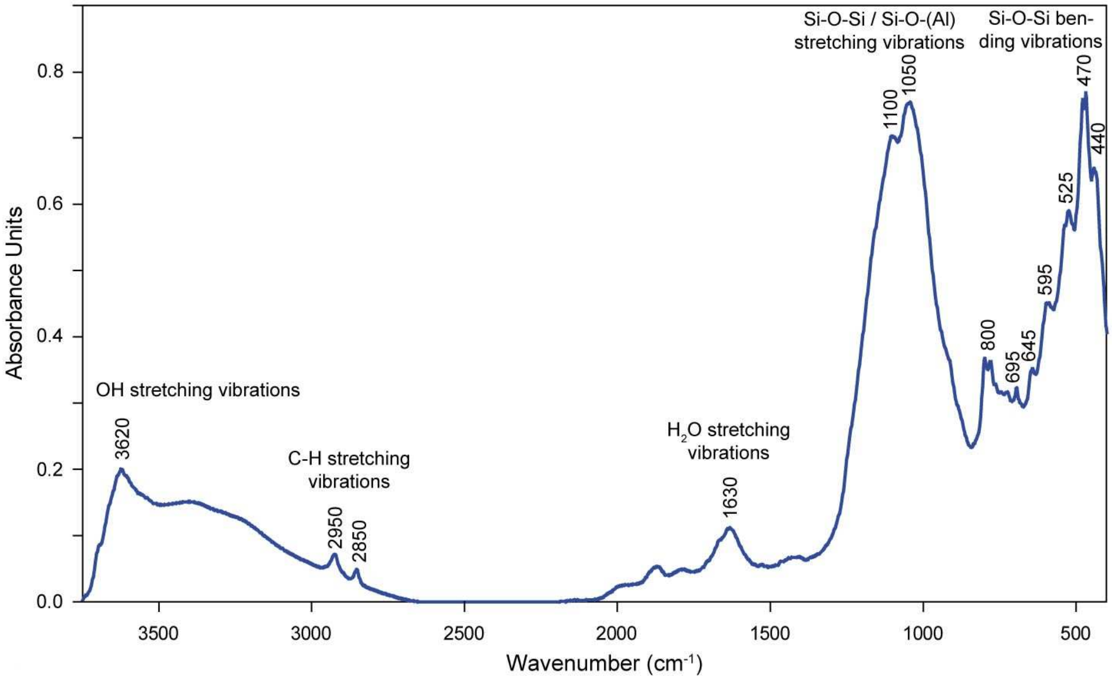

Figure 4.1 FTIR spectrum of a representative sediment sample from Lake El´gygytgyn in the wavenumber range of 400-3,750 cm^{-1}

Molecular vibrations of hydroxyl groups which are major components of clay minerals and opal ($SiO_2 \times nH_2O$), and a common functional group of organic substances are excited through absorption in the spectral region between 3,000 and 3,700 cm^{-1} (OH stretching) (Moenke 1974a; Kellner et al. 2004). Minerogenic compounds additionally show absorption bands of OH bending vibrations lying between 400 and 1,200 cm^{-1} (Moenke 1974a). In the spectrum of the sample from Lake El´gygytgyn, these regions are characterized respectively by absorbance of low to medium intensity and not determinable due to overlapping of absorption bands. The distinctive absorption peak at around 3,620 cm^{-1} can probably partly be related to defined OH stretching vibrations of clay minerals (Farmer 1974; Madejevá 2003; Pironon et al. 2003). Absorption bands characteristic for organic substances occur within the whole FTIR spectrum (KELLNER et al. 2004), but are hardly detectable due to the low TOC concentrations and the dominance of minerogenic compounds causing overlaps of spectral information. However, stretching vibrations in carbon hydrogen bonds exited through absorption at 2,850 and 2,950 cm^{-1} (MECOZZI and PIETRANTONIO 2006) are clearly visible in the spectrum of samples with higher TOC content. The absorption peak at around 1,630 cm^{-1} can be related to CO stretching vibrations of organic matter (MECOZZI and PIETRANTONIO 2006). Since the peak occurs in every FTIR spectrum, although the sample is almost free of organic substances, it is most likely mainly based on H-O-H bending vibrations of H_2O molecules (GENDRON-BADOU et al. 2003; PIRONON et al. 2003). Not chemically combined water probably arises from the adsorption of water by KBr. A more detailed assignment of defined absorption bands to certain compounds is very difficult due to the overlapping spectral information of several sediment compounds.

4.2 Calibration Models

4.2.1 Statistical Performance

The internal validation of the developed calibration models shows a strong correlation between conventionally measured and FTIRS-inferred concentrations of $TC_{(EA)}$ ($R^2_{cv} = 0.86$), $TC_{(LA)}$ ($R^2_{cv} = 0.82$), (TOC ($R^2_{cv} = 0.75$), TIC ($R^2_{cv} = 0.79$) and BSi ($R^2_{cv} = 0.96$) (see Table 4.1). Accordingly, the RMSECV are low with values of 0.09% for $TC_{(EA)}$ and $TC_{(LA)}$ (3.4%/3.2% of the gradient), 0.08% for TOC (2.8% of the gradient), 0.03% for TIC (2.1% of the gradient) and 2.7% for BSi (4.9% of the gradient). The correlation between conventionally measured and FTIRS-inferred TN concentrations is also statically significant, but is poorer ($R^2_{cv} = 0.61$) compared to the other developed models. The RMSECV of the TN model is 0.01% (5.9% of the gradient).

The results of the external model validation with high coefficients of determination between conventionally measured and FTIRS-inferred concentrations for $TC_{(EA)}$ ($R^2 = 0.90$), $TC_{(LA)}$ ($R^2 = 0.89$), TOC ($R^2 = 0.90$), TIC ($R^2 = 0.75$) and BSi ($R^2 = 0.92$) indicate a good prediction ability of the general trend by the calibration models (see Figure 4.2, Table A.2 and A.3 in the annex). Corresponding RMSEP for $TC_{(EA)}$ (0.11%, 7.4% of the gradient), $TC_{(LA)}$ (0.11%, 6.7% of the gradient), TOC (0.11%, 6.7% of the

Table 4.1 Statistical performance of calibration models from the composite profile of D1 for TC (conventionally measured with a vario MIRCRO cube element analyzer ($TC_{(EA)}$) and a DIMATOC 100 liquid analyzer ($TC_{(LA)}$)), TOC, TIC, TN and BSi including the number of components, samples and wavelength ranges used in the models, descriptive statistics of the calibration set and the validation set, the number of removed outliers, the cross validated coefficient of determination (R^2_{cv}) (conventionally vs. FTIR-inferred concentrations), the root mean square error of cross validation (RMSECV (absolute and percentage of the gradient of the calibration set)), the coefficient of determination (conventionally vs. FTIR-inferred concentrations), and the root mean square error of prediction (RMSEP (absolute and percentage of the gradient of the validation set))

Statistics		$TC_{(EA)}$ (%)	$TC_{(LA)}$ (%)	TOC (%)	TIC (%)		TN (%)	BSi (%)	
		all WL	all WL	all WL	all WL	selected WL	all WL	all WL	selected WL
calibration set	PLS components	10	10	11	10	8	6	3	4
	Samples (*n*)	144	150	152	151	151	145	132	132
	Min	0.07	0.12	0.02	0.01	0.01	0.00	0.9	0.9
	Max	2.72	2.95	2.89	1.46	1.46	0.17	56.5	56.5
	Gradient	2.65	2.83	2.87	1.45	1.45	0.17	55.6	55.6
	Mean	0.42	0.45	0.33	0.12	0.12	0.05	16.5	16.5
	Wavelengths included (cm^{-1})	400-3,750	400-3,750	400-3,750	400-3,750	700-725; 860-890; 1,300-1,560; 1,780-1,810; 2,460-2,640	400-3,750	400-3,750	1,050-1,250
	Outliers removed	3	3	1	2	2	2	1	1
internal validation	R^2_{cv}	0.86	0.82	0.75	0.79	0.89	0.61	0.96	0.95
	RMSECV	0.09	0.09	0.08	0.03	0.03	0.01	2.7	3.2
	RMSECV (% gradient)	3.4	3.2	2.8	2.1	2.1	5.9	4.9	5.8
validation set	Min	0.05	0.08	0.04	0.02		0.00	1.2	
	Max	1.54	1.73	1.68	0.40		0.11	36.9	
	Gradient	1.49	1.65	1.64	0.38		0.11	35.7	
	Mean	0.39	0.46	0.37	0.09		0.04	10.1	
external validation	R^2	0.90	0.89	0.90	0.75	0.89	0.61	0.92	0.91
	RMSEP	0.11	0.11	0.11	0.07	0.03	0.02	2.5	2.9
	RMSEP (% gradient)	7.4	6.7	6.7	18.4	7.9	18.2	7.0	8.1

WL - Wavelengths

gradient), TIC (0.07%. 18.4% of the gradient) and BSi (2.5%, 7.0% of the gradient) show a moderate to good prediction accuracy with respect to the absolute values. The poorer statistical performance of the FTIR-TN model affects the prediction ability of the general trend and the absolute values. Therefore, the R^2 of 0.61 is moderate and the RMSEP of 0.02% (18.2% of the gradient) is high compared to the other calibration models. The higher number of PLS components (8-11) used for both TC models; the TOC model and the TIC model indicates a higher complexity of the corresponding models compared to the models for TN and BSi with a lower number of components (3-6).

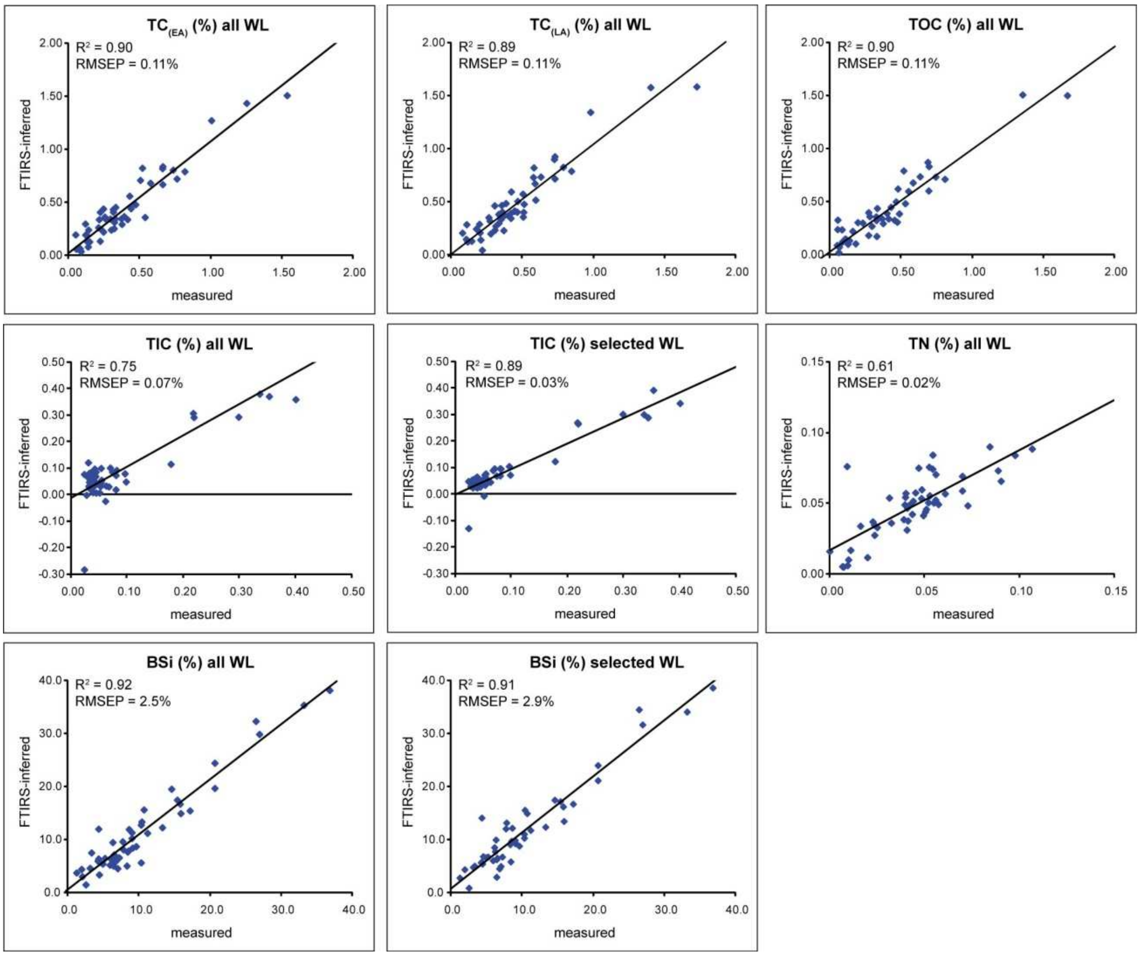

Figure 4.2 Scatter plots of conventionally measured (x-axis) versus FTIRS-inferred by models from the composite profile of D1 (y-axis) concentrations for $TC_{(EA)}$, $TC_{(LA)}$, TOC, TIC, TN, and BSi showing the results of the external validation. Models are based on the entire wavelength range (all WL) or on wavelengths specific to the property of interest (selected WL).

ROSÉN et al. (2010) have shown that it is possible to establish robust FTIRS calibration models solely based on certain wavelengths which are strongly related to the biogeochemical property of interest. Wavelength related to C-O molecular vibrations of calcite (700-725, 860-890, 1,300-1,560, 1,780-1,810, 2,460-2,640 cm^{-1}) and wavelength related to diatoms (biogenic silica) (1,050-1,250 cm^{-1}) (ROSÉN et al. 2010) were used for TIC and BSi calibration models. The statistical performance of the FTIR-TIC model shows higher R^2_{cv} and R^2 (0.89) compared to the TIC model based on all wavelengths. The corresponding RMSECV are equal in both models (0.03%, 2.1% of the gradient), while the RMSEP is lower in the modified TIC model (0.03%, 7.9% of the gradient). The modified FTIR-BSi model has an R^2_{cv} of 0.95, an R^2 of 0.91, an RMSECV of 3.2% (5.8% of the gradient), and an RMSEP of 2.9% (8.1% of the gradient). Hence, the statistical performance of this model is slightly poorer than that of the BSi model including all wavelengths.

Importance of the Conventional Measurement

Since the calibration of the FTIR models is based on conventional measurements, it is necessary to minimize the measurement error to yield a high accuracy in the prediction of certain biogeochemical property concentrations. An interlaboratory comparison of the biogenic silica measurements by CONLEY (1998) has shown that the percent standard deviation of the mean varies between 67.5% for low concentrations (BSi = 1.31%) and 21.2% for high concentrations (BSi = 44.3%). In this study, a percent standard deviation of the mean of 20.3% (3.9±0.8 wt%), 10.4% (10.4±1.2 wt%) and 12.2% (17.3±2.1 wt%) was calculated for three samples of different BSi concentration based on 17 repetitions for each sample. With regard to these results, multiple measurements were applied to 65 of the 132 samples from the calibration set to test if multiple measurements improve the statistical performance of the BSi model. A calibration model (including all wavelengths) for BSi only based on single measurements has an R^2_{cv} of 0.94, an RMSECV of 3.2% (5.8% of the gradient), an R^2 of 0.90, and an RMSEP of 3.0% (8.4% of the gradient), while the model including multiple measurements has an R^2_{cv} of 0.96, an RMSECV of 2.7% (4.9% of the gradient), an R^2 of 0.92, and an RMSEP of 2.5% (7.0% of the gradient). Thus, the application of multiple measurements improved all assessment criteria of the BSi model. The R^2_{cv} and the R^2 are slightly increased (about 0.02), whereas the RMSECV and the RMSEP are slightly reduced (about 0.5%). The relatively high inaccuracy of the conventional method and the possible consequential decrease of the statistical performance of the BSi calibration model demonstrate the importance of reliable conventional measurements and the potential of multiple measurements. The examination of the other biogeochemical property measurements might be reasonable as well, in this respect.

4.2.2 Relationship between FTIRS Models and Biogeochemical Properties

FTIR-BSi model

The loadings of the PLS component 1 of the calibration model for the inference of BSi concentrations show positive values in the spectral regions from 470-500, 780-880, 1,065-1,300, and 2,700-3,560 cm^{-1}, while negative values are situated in the regions from 400-470, 500-780, 880-1,065, 1,300-2,700, and 3,560-3685 cm^{-1} (see Figure 4.3). The wavelengths explaining most of the spectral variation depending on the primary data values lie between 1,065 and 1,300 cm^{-1} and are strongly positive. This indicates a positive correlation to the BSi concentrations. This region and the two slightly positive bands from 470-500 and 780-880 cm^{-1} can be related to the characteristic molecular vibrations of biogenic silica. Absorption at around 475 cm^{-1} is caused by bending vibration modes of Si-O-Si. Absorptions at around 800 cm^{-1} are attributed to inter-tetrahedral Si-O-Si bending vibration modes, while absorption at around 1,100 cm^{-1} can be assigned to stretching vibration modes of the SiO_4 tetrahedron (MOENKE 1974b; GENDRON-BADOU et al 2003). These findings are supported by the FTIR spectrum of a diatom sample (purity >96%) from Lake El´gygytgyn showing distinctive absorption bands from 430-490, 780-830 and 1,040-1,250 cm^{-1} (see Figure 4.4). A fourth lower absorption peak centered at 940 cm^{-1} is also observable in the spectrum and corresponds well with known Si-OH molecular vibrations for biogenic silica (RICKERT et al. 2002; GENDRON-BADOU et al. 2003). However, the loadings of the BSi model are strongly negative in this region. The entire spectral region between 400 and 1,065 cm^{-1} is mainly dominated by negative loading values, especially in the regions from 500-620 and 915-1,065 cm^{-1}. Other silicates like feldspar, quartz and clay minerals absorb in this part of the FTIR spectrum as well and cause an overlapping of absorption bands. The influence of this region on the loadings of the BSi calibration model indicates that direct relationships as well as indirect relationships to the BSi concentrations are considered in the model. This can be explained by the fact that measurements of biogeochemical property concentrations reflect the relative proportion of biogeochemical and minerogenic compounds. Thus, the absorption peak at 940 cm^{-1} is overlapped by absorption bands of other silicates negatively correlated to the concentration of BSi. The positive loading values in the spectral regions between 2,700 and 3,560 cm^{-1} can be linked to stretching vibrations of OH molecules (MOENKE 1974a), which are major components of biogenic silica. The effect of chemically bond water is also observable in the spectrum of the diatom sample as absorbance of medium intensity in the spectral region between 3,000 and 3,700 cm^{-1}. OH stretching vibrations of clay minerals might explain the negative loading values in the wavelength range 3560-3685 cm^{-1} (FARMER 1974; MADEJEVÁ 2003; PIRONON et al. 2003).

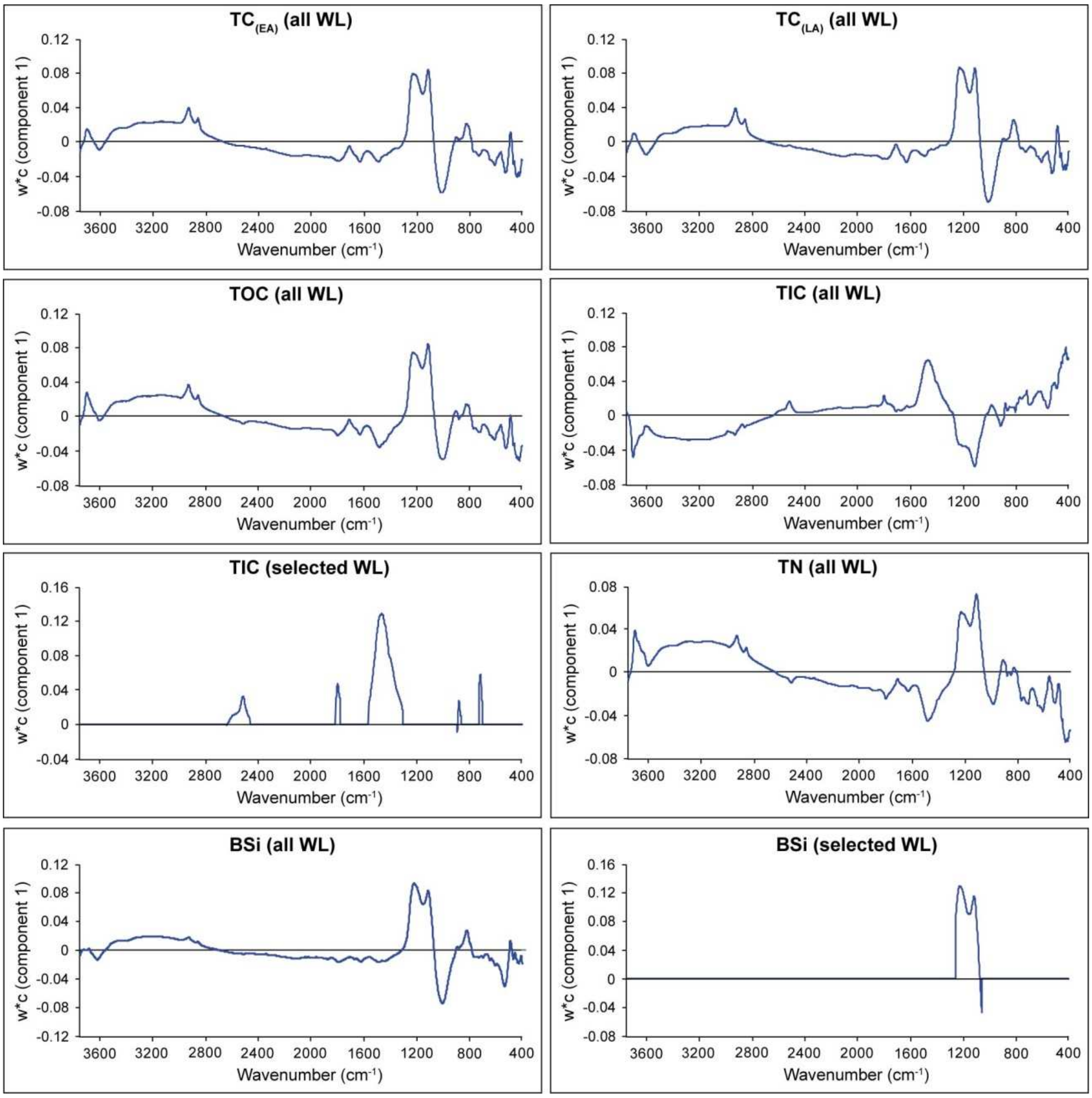

Figure 4.3 Loading plots of the developed FTIRS models from the composite profile of D1 for $\mathrm{TC}_{(EA)}$, $\mathrm{TC}_{(LA)}$, TOC, TIC, TN, and BSi showing the contribution of each wavenumber to the PLSR model. Positive values indicate wavenumbers positively correlated to the property of interest and negative values indicate wavenumbers negatively correlated to the property of interest. Loadings are expressed by weight vectors (w*c) of the PLSR model (component 1) (y-axis) and the corresponding wavelength range (x-axis). Models are based on the entire wavelength range (all WL) or on wavelengths specific to the property of interest (selected WL).

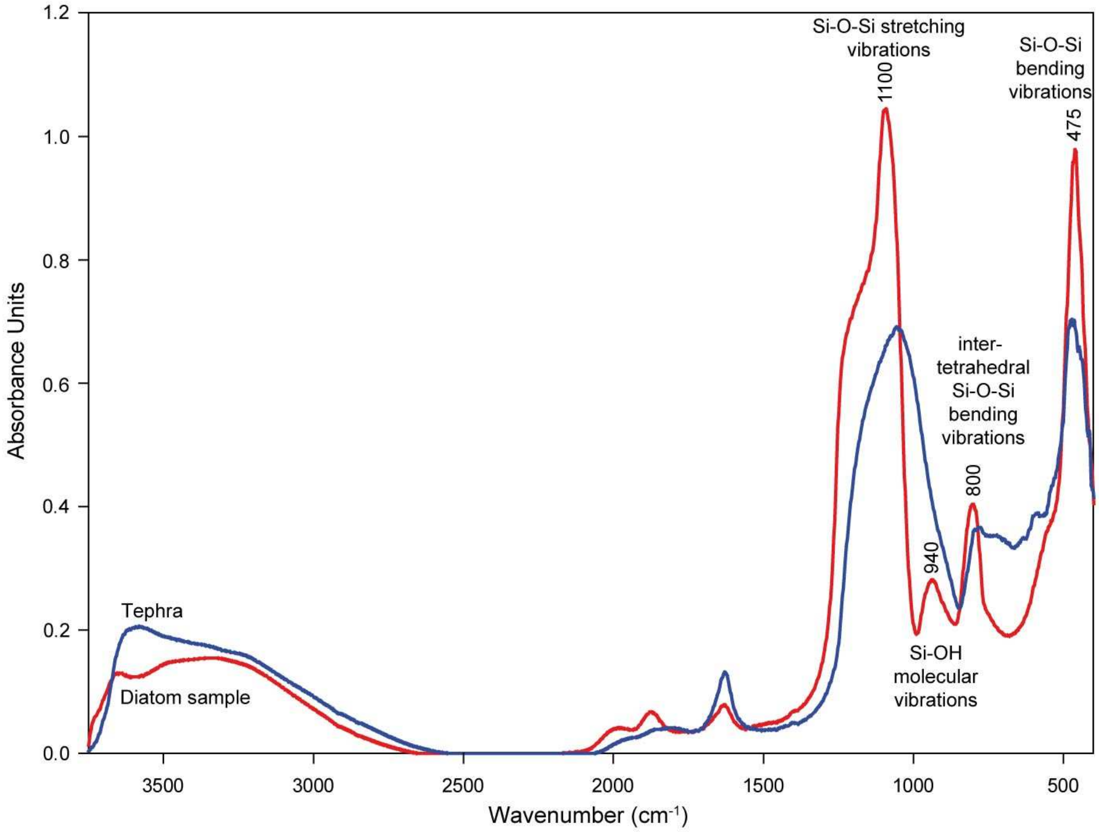

Figure 4.4 FTIR spectra of a tephra sample (blue line) and a diatom sample (purity >96%) (red line) from Lake El´gygytgyn.

A comparison between FTIR spectra of samples from Lake El´gygytgyn with different BSi concentrations shows that the increase of the absorption peak at 1100 cm^{-1} compared to the peak at 1050 cm^{-1} corresponds well with increasing BSi content (see Figure 4.5). The assumption of VOGEL et al. (2008) and ROSÉN et al. (2010) that the absorption band centered at 1,100 cm^{-1} is the most important band for the FTIR-BSi model is confirmed by the findings of this study. Other distinctive absorption peaks related to biogenic silica are strongly affected by spectral overlaps due to absorption of other silicates. However, it has to be taken into account that other minerals, e.g. quartz, show absorption in the IR region between 1,050 and 1,250 cm^{-1} as well (MOENKE 1974b). The fact that the inclusion of only this spectral region to the calibration model does not yield a better statistical performance compared to the BSi model based on all wavelengths (see Section 4.2.1) highlights the importance of indirect relationships.

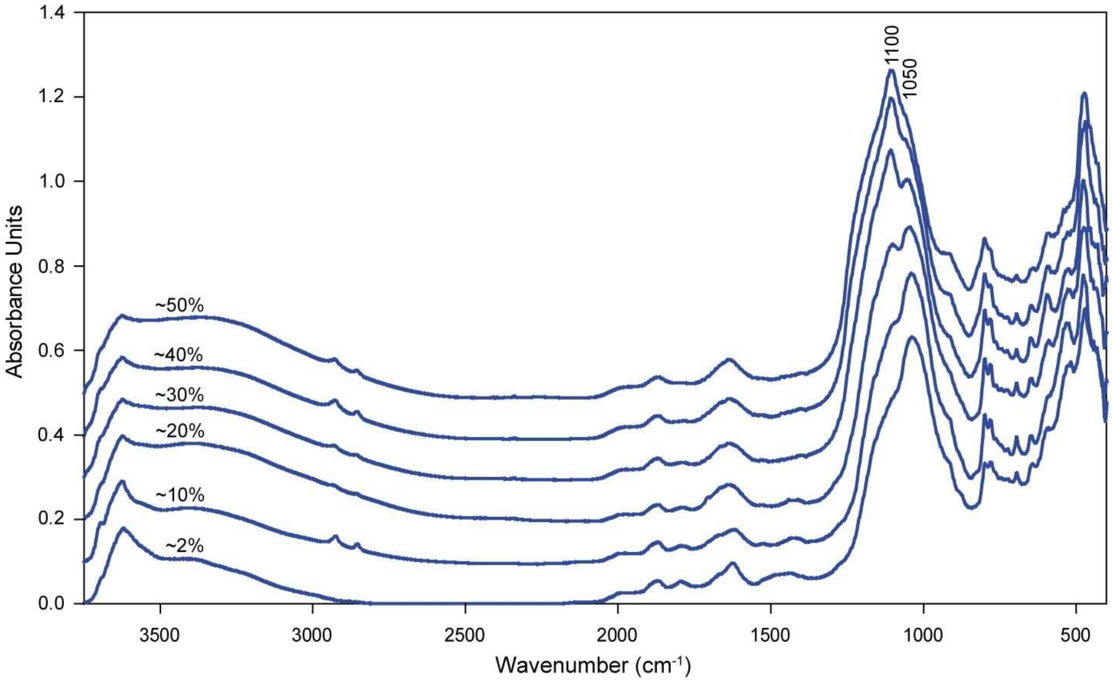

Figure 4.5 FTIR spectra of sediment samples from Lake El´gygytgyn with different BSi concentrations (~2%, ~10%, ~20%, ~30%, ~40%, ~50%) showing an increase of the absorption peak at 1,100 cm^{-1} with increasing BSi concentrations. Spectra were shifted vertically for better visualization.

The FTIR spectrum of a tephra layer from Lake El´gygytgyn shows strong similarities to the spectrum of a diatom sample (see Figure 4.4). This suggests that opal of volcanic origin has a negative impact on the prediction of biogenic silica concentrations in the form of overestimated BSi values, although the maximum absorption peak of the tephra is shifted from 1100 to 1050 cm^{-1} compared to the peak of biogenic silica. This impact might be enhanced by using a calibration model solely based on a certain spectral region, since in this case only the part of the IR spectrum with positive loading values in the PLS component 1 of the BSi model is considered.

FTIR-TC and –TOC Model

The wavelengths of the calibration models for TC and TOC are very similar. This is a result of the predomination of organic carbon compared to inorganic carbon in the sediment record of Lake El´gygytgyn. The loading values of the PLS component 1 for the TC_{EA}, TC_{LA} and TOC model are positive in the spectral region from 1,065-1,300 and 2,700-3,550 and at around 480, 810 and 3,700 cm^{-1} which indicates a positive correlation to the biogeochemical property concentrations (see Figure 4.3). Negative loading values dominate the spectral regions from 400-1,065, 1,300-2,700 and around 3,600 cm^{-1}. The strongest absorption band of the three models is situated between 1,065 and 1,300 cm^{-1} and shows two discrete peaks at 1,100 and 1,220 cm^{-1}. Absorption of IR radiation in this region can be linked to known absorption bands of organic compounds. For instance, absorptions between 1,040 and 1,070 cm^{-1} are ascribed to C-O stretching vibrations of carbohydrates or polysaccharides (Calace et al. 1999; Chapman et al. 2001; Cocozza et al. 2003). Absorptions at around 1,125 cm^{-1} are due to C-O-C stretching vibrations of complex carbohydrates and absorption between 1,230 and 1,265 cm^{-1} are attributed to C-O stretching vibrations of ethers or carboxyl groups (Cocozza et al. 2003; Mecozzi and Pietrantonio 2006).

An alternative explanation for the importance of the spectral region between 1,065 and 1,300 cm^{-1} is based on relationships between the TC/TOC concentration and the BSi content. Since the loading plots for the TC and TOC model show apparent similarities to the loadings of the BSi model, it is likely that both models are affected by the content of BSi, which clearly exceeds the carbon concentrations in the sediment record of Lake El´gygytgyn. The possible influence of one property on the other properties is reflected by moderate correlations (R^2 = 0.53-0.62) between the biogeochemical properties (see Table 4.2). Therefore, it is likely that this part of the IR spectrum is mainly related to Si-O molecular vibrations of biogenic silica and only partly connected to the concentration of certain organic compounds. This assumption might also explain the slightly positive loading values in the spectral region from 470-495 and 775-915 cm^{-1}, which can be ascribed to Si-O molecular vibrations of biogenic silica as well (Moenke 1974b; Gendron-Badou et al 2003).

Table 4.2 Correlation between the biogeochemical properties of the calibration set of D1 indicated by the coefficient of determination (R^2)

	TC_{EA}/TC_{LA}	TC_{EA}/TOC	TC_{LA}/TOC	TC_{EA}/TN	TC_{LA}/TN
R^2	0.96	0.84	0.81	0.42	0.29
	TOC/TN	TC_{EA}/BSi	TC_{LA}/BSi	TOC/BSi	TN/BSi
R^2	0.56	0.59	0.53	0.62	0.52

Positive loading values between 2,800 and 3,000 cm^{-1} with distinct peaks at 2,850 and 2,930 cm^{-1} can be attributed to stretching vibrations of C-H molecules in $-CH$, $-CH_2$ and $–CH_3$ groups of aliphatic and protein chains (Chapman et al. 2001; Cocozza et al.

2003; MECOZZI and PIETRANTONIO 2006). The positive values between 2,700 and 3,500 cm^{-1} as well as at around 3,700 cm^{-1} are related to absorptions caused by hydroxide groups. OH molecules are common in organic matter. However, since the influence of BSi on the calibration models for TC and TOC is likely, it is difficult to determine how much of the absorption is caused by hydroxide contained in organic matter (direct relationship) and how much of the absorption results from hydroxide groups associated with BSi (indirect relationships). The negative loading values between 400 and 1,065 cm^{-1} and at around 3,600 cm^{-1} can be ascribed to SiO molecular vibrations of silicates and to vibrations of OH molecules contained in silicates, e.g. in clay minerals. The negative character of this spectral region can be explained by the indirect relationship arising from the measurement of the relative proportion between carbon and minerogenic components of the sediment. A further determination of absorption bands of certain organic compounds cannot be made due to the spectral overlapping of multiple bands resulting from other sediment components, particularly from minerogenic matter.

Anti-correlated peaks, especially observable in the loading plot of the TOC model, between 1,380-1,540, at around 1,790 and 2510 cm^{-1} are related to absorption bands of inorganic carbon (HUANG and KERR 1960; WHITE 1974; MECOZZI et al. 2001). The negative character of these peaks can be explained by the simultaneous occurrence of TIC with almost solely low concentrations of TC and particularly of TOC.

FTIR-TIC Model

The loadings values of the PLS component 1 of the calibration model for TIC are positive in the spectral region from 400-885, 940-1,025 and 1,270-2,630 cm^{-1}, while negative values appear from 885-940, 1,025-1,270 and 2,630-3,730 cm^{-1} (see Figure 4.3). Distinctive absorption peaks at around 715, 875, 1795, 2515 cm^{-1} and a broad absorption band around 1460 cm^{-1} correspond well with known spectral regions related to molecular vibrations of carbonates (HUANG and KERR 1960; WHITE 1974; MECOZZI et al. 2001). Furthermore, FTIRS model developments by VOGEL et al. (2008) and ROSÉN et al. (2010) as well as FTIR spectra of carbonate-rich sediments (ROSÉN et al. 2010) have also shown that these spectral regions are the most important for carbonates.

The negative loading values between 1,025 and 1,270 cm^{-1} with an distinctive peak at around 1,100 cm^{-1} as well as the negative values between 2,630 and 3,730 cm^{-1} can partly be explained by an indirect relationship between the occurrence of TIC and BSi. The above-mentioned wavelength ranges are strongly related to Si-O molecular vibrations of BSi and to vibrations of hydroxide groups contained in BSi, respectively. Due to the fact TIC almost only appears in the lowermost part of the composite record from Lake El´gygytgyn, which is also dominated by low concentrations of BSi, it is likely that the importance of those spectral regions is depending on this correlation. A second explanation for the anti-correlation of the IR range from 2,630-3,730 cm^{-1} might be the effect of diagenesis, particularly the effect of compaction, on the sediments of Lake El´gygytgyn (see Section 4.5). It is supposable that the influence of these processes yields a release of chemically combined water with increasing burial depth, where TIC begins to occur. The positive loading values from 400-885 and 940-1,025 cm^{-1} can be assigned to Si-O molecular vibrations of silicates. The positive character of this range is probably based on the correlation between the occurrence of TIC and the domination of minerogenic compounds.

The TIC calibration model based on wavelengths specific for carbonates has a better statistical performance than the model based on all wavelengths (see Section 4.2.1). This shows that, in contrast to the calibration model for BSi, indirect relationships have a negative effect on the prediction of TIC concentrations. However, in this case the indirect relationships depend on the special composition of the sediment record with an occurrence of TIC almost only in the lowermost part.

FTIR-TN Model

The loading values of the calibration model for TN show similarities to the loading plots of the models for BSi, TC, TOC and TIC. Therefore, they cannot be assessed independently, as already presumed by VOGEL et al. (2008). Positive loading values are situated in the spectral regions from 800-835, 880-930, 1,050-1,275 and 2,640-3,730 cm^{-1}, whereas the spectral ranges from 400-800, 835-880, 930-1,050 and 1,275-2,640 cm^{-1} show negative values (see Figure 4.3). None of the observable peaks can be related to specific absorption bands of bonds including nitrogen. For instances, absorption bands at around 1,550 cm^{-1} are known to be ascribed to –NH bending vibrations and –CN stretching vibrations (COCOZZA et al. 2003; MECOZZI and PIETRANTONIO 2006). The loading plot of the PLS component 1 for the TN model is affected by several indirect relationships. Analogies to the loadings of the TOC model can be explained by the linkage of nitrogen to organic compounds, since nitrogen plays a major role in the composition of organic matter. This linkage is expressed by a moderate R^2 for the correlation between TN and TOC of 0.56 for the samples in the calibration set. The dependence of TN on TOC can be seen in the loadings of both models by the absorption band between 2,800 and 3,000 cm^{-1}, which is assigned to -CH, $-CH_2$ and $–CH_3$ groups and is similarly developed in the TOC as well as in the TN model. The strongly positive loadings between 1,050 and 1,275 cm^{-1} in the loading plot of the TN mode can be related to Si-O molecular vibrations of BSi. This can probably be explained by the moderate correlation between TN and BSi ($R^2 = 0.52$). Moreover, the distinguishable anti-correlated peaks at around 1,470, 1,800, 2,510 cm^{-1} are likely due to molecular vibrations in carbonates. The effect of TIC on the TN calibration model results from the coincident occurrence of very low TN and TIC values.

The non-detectable absorption bands related to TN and the strong effect of indirect relationships on the calibration model make it very difficult to reasonably assess the loading plot of the TN model. Due to this fact and the merely moderate statistical performance of the TN calibration model (see Section 4.2.1), it is recommendable to apply the model in consideration of these circumstances.

4.3 Comparison between FTIR Models based on the Sediments of D1 and FTIR Models derived from the Sediments of Core Lz1024

FTIRS calibration models derived from core Lz1024 (H. VOGEL, unpublished data) are based on the uppermost 16.60 m of the sediment record of Lake El´gygytgyn with an approximately age of 340 ka (MELLES et al. 2009), while the FTIRS models derived from the composite profile of D1 include the entire sediment record (~315 m) with an age about 3.6 Ma. The results of the internal validation of the models from Lz1024 are comparable to those resulting from the internal validation of the models from D1 and show strong correlations between the conventional and FTIRS-inferred biogeochemical property concentrations (see Table 4.3). The resulting R^2_{cv} for the Lz1024 models amount to 0.84 for TC, 0.81 for TOC, 0.76 for TN, and 0.74 for BSi, while the corresponding RMSECV are low with values of 0.15% (6.4% of the gradient) for TC, 0.17% (7.1% of the gradient) for TOC, 0.01% (3.3% of the gradient) for TN and 1.9% (7.4% of the gradient) for BSi. The external validation uses the 50 samples of the validation set which are distributed over the whole composite profile of D1. In contrast to the internal validation, this external validation shows a poorer statistical performance of the models from Lz1024 compared to the models of D1. The prediction ability of general trend and absolute values is lower. The R^2 resulting from the correlation between conventional and FTIRS-inferred values indicating the prediction ability of the general trend are still significant for TC and BSi with values of 0.69 and 0.84. Values of 0.42 and 0.43 for TOC and TN demonstrate less reliable prediction abilities (see Figure 4.6, Table A.2 and A.4 in the annex). The prediction accuracy relative to the absolute values assed by the RMSEP is low for all considered biogeochemical properties. Corresponding RMSEP are 0.64% (43.0% of the gradient) for TC, 0.73% (44.5% of the gradient) for TOC, 0.08% (72.7% of the gradient) for TN, and 4.9% (13.7% of the gradient) for BSi. A minor part of the higher divergence between FTIRS-inferred values by models of core Lz1024 and conventionally measured values compared to concentrations inferred by models of D1 can be explained by differences in the measuring methods and devices used for the determination (see Section 3.1.2). The higher RMSEP of the BSi model from core Lz1024 partly results from the fact that the calibration range of the model does not cover the lowest (three samples below 2.1%) and the highest concentrations (two samples above 27.9%) included in the validation set.

Table 4.3 Comparison of the statistical performance of the FTIRS models for TC, TOC, TN and BSi derived from the composite profile of D1 and core Lz1024 including the number of components, samples and wavelength ranges used in the models, descriptive statistics of the calibration set and the validation set, the number of removed outliers, the cross validated coefficient of determination (R^2_{cv}) (conventionally vs. FTIR-inferred concentrations), the root mean square error of cross validation (RMSECV (absolute and percentage of the gradient of the calibration set)), the coefficient of determination (conventionally vs. FTIR-inferred concentrations), and the root mean square error of prediction (RMSEP (absolute and percentage of the gradient of the validation set))

Statistics		TC[1] (%)		TOC (%)		TN (%)		BSi (%)	
		D1	Lz1024	D1	Lz1024	D1	Lz1024	D1	Lz1024
calibration set	PLS components	10	8	11	8	6	9	3	3
	Samples (*n*)	144	1657	152	1657	145	1657	132	201
	Min	0.07	0.01	0.02	0.03	0.00	0.00	0.9	2.1
	Max	2.72	2.37	2.89	2.41	0.17	0.30	56.5	27.9
	Gradient	2.65	2.36	2.87	2.38	0.17	0.30	55.6	25.8
	Mean	0.42	0.58	0.33	0.66	0.05	0.08	16.5	9.1
	Wavelengths included (cm^{-1})	400-3,750	400-3,750	400-3,750	400-3,750	400-3,750	400-3,750	400-3,750	400-3,750
	Outliers removed	3	-	1	-	2	-	1	4
internal validation	R^2_{cv}	0.86	0.84	0.75	0.81	0.61	0.76	0.96	0.74
	RMSECV	0.09	0.15	0.08	0.17	0.01	0.01	2.7	1.9
	RMSECV (% gradient)	3.4	6.4	2.8	7.1	5.9	3.3	4.9	7.4
validation set	Min	0.05		0.04		0.00		1.2	
	Max	1.54		1.68		0.11		36.9	
	Gradient	1.49		1.64		0.11		35.7	
	Mean	0.39		0.37		0.04		10.1	
external validation	R^2	0.90	0.69	0.90	0.42	0.61	0.43	0.92	0.84
	RMSEP	0.11	0.64	0.11	0.73	0.02	0.08	2.5	4.9
	RMSEP (% gradient)	7.4	43.0	6.7	44.5	18.2	72.7	7.0	13.7

[1] Results of the element analyzer (TC_{EA}) were used for the TC model of D1

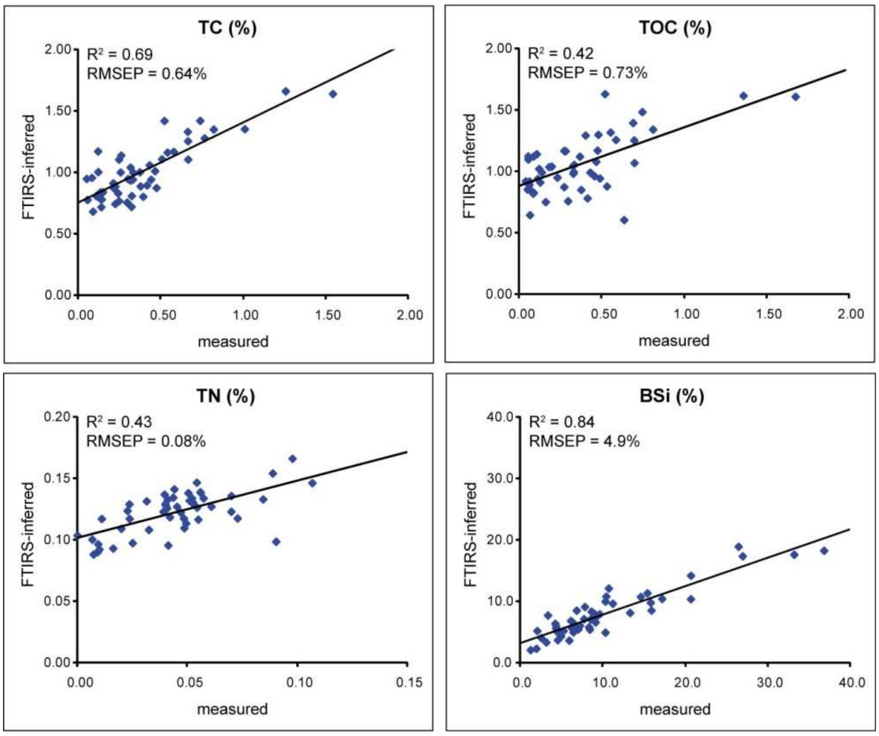

Figure 4.6 Scatter plots showing the results of the external validation of the models from core Lz1024. Concentrations of TC, TOC, TN, and BSi conventionally measured (x-axis) versus FTIRS-inferred by models from core LZ1024 (y-axis).

FTIR-BSi Model

The comparison between the loadings of the PLS component 1 of the BSi models derived from the sediments of core Lz1024 and D1 shows a similar pattern in both models (see Figure 4.7). The wavelength range between 1,050 and 1,300 cm^{-1} in both cases has strong positive loading values and therefore explains most of the spectral variations depending on the primary data. This range is related to SiO molecular vibrations of biogenic silica. Furthermore, the spectral region between 400 and 1,050 cm^{-1} is mainly negatively correlated to the BSi concentration in both models. However, the values of the peaks at around 815 and 990 cm^{-1} are more positively and more negatively developed, respectively, in the model based on the entire sediment record. Moreover, the slightly positive loading peak at around 470 cm^{-1} in the loadings of this model is shifted to lower wavenumbers at around 450 cm^{-1} in the model from core Lz1024. The wavelength range between 2,700 and 3,500 cm^{-1} which can be attributed to molecular vibrations of hydroxide is not weighted in the BSi model from core Lz1024 in contrast to the model from D1.

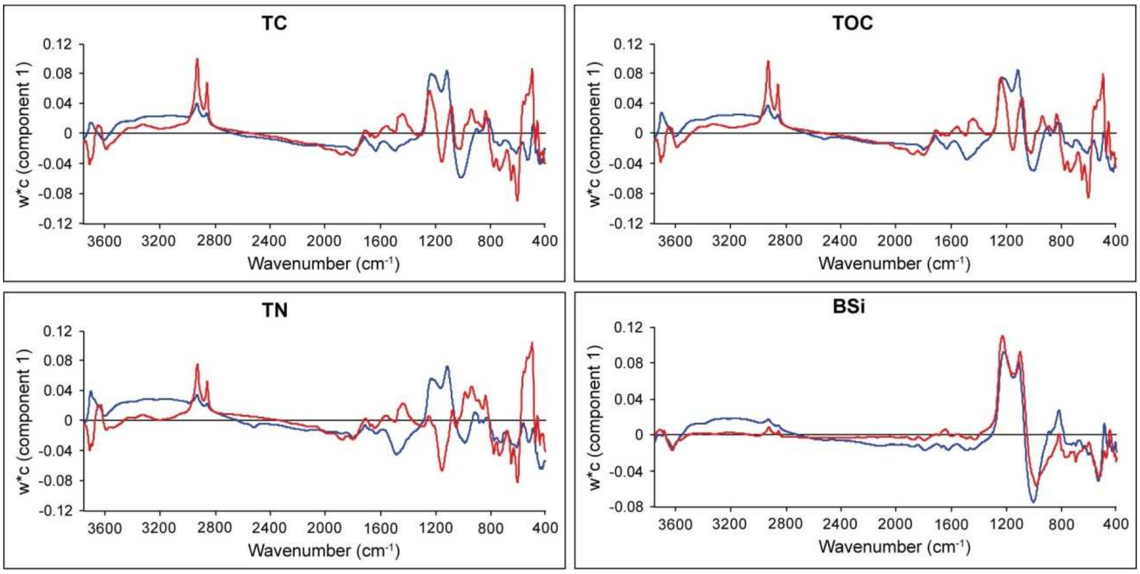

Figure 4.7 Loading plots of the FTIRS models from the composite profile of D1 (blue line) and from core Lz1024 (red line) for TC, TOC, TN, and BSi showing the contribution of each wavenumber to the PLSR model. Positive values indicate wavenumbers positively correlated to the property of interest and negative values indicate wavenumbers negatively correlated to the property of interest. Loadings are expressed by weight vectors (w*c) of the PLSR model (component 1) (y-axis) and the corresponding wavelength range (x-axis).

FTIR-TC/TOC/TN Model

Due to the strong similarities of the calibration models for TC[1], TOC and TN, these models were assessed together. The loadings of the PLS component 1 of the calibration models derived from the sediments of core Lz1024 (further referred as ‘Lz1024 models’) clearly differ from the loadings of models based on the sediments of D1 (further referred as ‘D1 models’) (see Figure 4.7). In contrast to D1 models, the loadings of the Lz1024 models can be related more clearly to absorptions of organic matter. The positive loading values in the spectral region from 1,055-1,115, 1,180-1,280, 1,370-1,470, and 1,520-1590 cm^{-1} can possibly be attributed to CO stretching vibrations of carbohydrates or polysaccharides, to CO stretching vibrations of ethers or carboxyl groups, to OH deformation vibrations of phenolic and aliphatic groups, and to NH bending and CN stretching vibrations of proteins (Amide I band) (Calace et al. 1999; Chapman et

---

[1] The TC calibration model derived from the sediments of D1 is based on the results of the element analyzer (TC_{EA}) and was used for the comparison with the TC model from core Lz1024, since the TC concentrations in core Lz1024 were also determined with this method.

al. 2001; COCOZZA et al. 2003; MECOZZI and PIETRANTONIO 2006). These spectral ranges are negative, overlapped by absorptions of other sediment compounds or not detectable in the loadings of the D1 models. The absorption band between 2,800 and 3,000 cm^{-1} which is linked to stretching vibrations of C-H molecules in -CH, -CH_2 and –CH_3 groups of aliphatic and protein chains (CHAPMAN et al. 2001; COCOZZA et al. 2003; MECOZZI and PIETRANTONIO 2006) has a considerably stronger effect on the Lz1024 models than on the D1 models. Particularly the loading pattern in the spectral region from 400 to 1,300 cm^{-1} which is ascribed to SiO molecular vibrations of silicates shows large differences in the models from core Lz1024 and D1. The loading values of the Lz1024 models are strongly positive from 480 to 570 cm^{-1} and strongly negative from 570 to 805 cm^{-1} in contrast to the D1 models where the loadings show strongly negative values in the spectral region between 900 and 1,050 cm^{-1}. In the loadings of the D1 models, the influence of the most important absorption band for BSi between 1,050 and 1,300 cm^{-1} is observable. This is not the case in the loadings of the Lz1024 models. In these models, the mentioned spectral range is subdivided in positive loading values from 1,055-1,115 and 1,180-1,280 cm^{-1} as well as in negative values between 1,115 and 1,180 cm^{-1}. The positive values can be linked to absorption of organic matter as described above and the negative values might be connected to absorptions of SiO molecules contained in silicates (e.g. quartz). Compared to the model for TC and TOC, the regions with positive loadings within this spectral range are negligible in the model for TN. The D1 models are strongly affected by the concentrations of BSi, whereas the Lz1024 models are apparently independent from this proxy. This can be explained by low correlations between TC, TOC, TN and BSi (R^2 = 0.09-0.21) for core Lz1024 compared to the correlations within the samples of the calibration set for D1 (R^2 = 0.52-0.62) (see Table 4.2 and 4.4).

Table 4.4 Correlation between the biogeochemical properties of the calibration set of core Lz1024 indicated by the coefficient of determination (R^2)

	TC/TOC	TC/TN	TC/BSi	TOC/TN	TOC/BSi	TN/Bsi
R^2	0.93	0.74	0.16	0.69	0.21	0.09

A down-core plot of the biogeochemical proxies of the samples from the validation set highlights the high prediction accuracy with respect to the general trend and the absolute values of the concentrations inferred by models based on samples from the entire sediment record of Lake El´gygytgyn (see Figure 4.8). BSi concentrations inferred by the calibration model of Lz1024 significantly match the conventional concentrations as well. However, high BSi concentrations are constantly underestimated by the model due to the insufficient calibration in the range above 20% which is only covered by four samples with a maximum value of 27.9%. In contrast to this model, the FTIR models for TC, TOC, and TN derived from core Lz1024 considerably overestimated the biogeochemical property concentrations throughout the validation set. Furthermore, a slight increase in the difference between conventionally and FTIRS-inferred values with increasing sample depth can be observed for these models. These divergences and the dif-

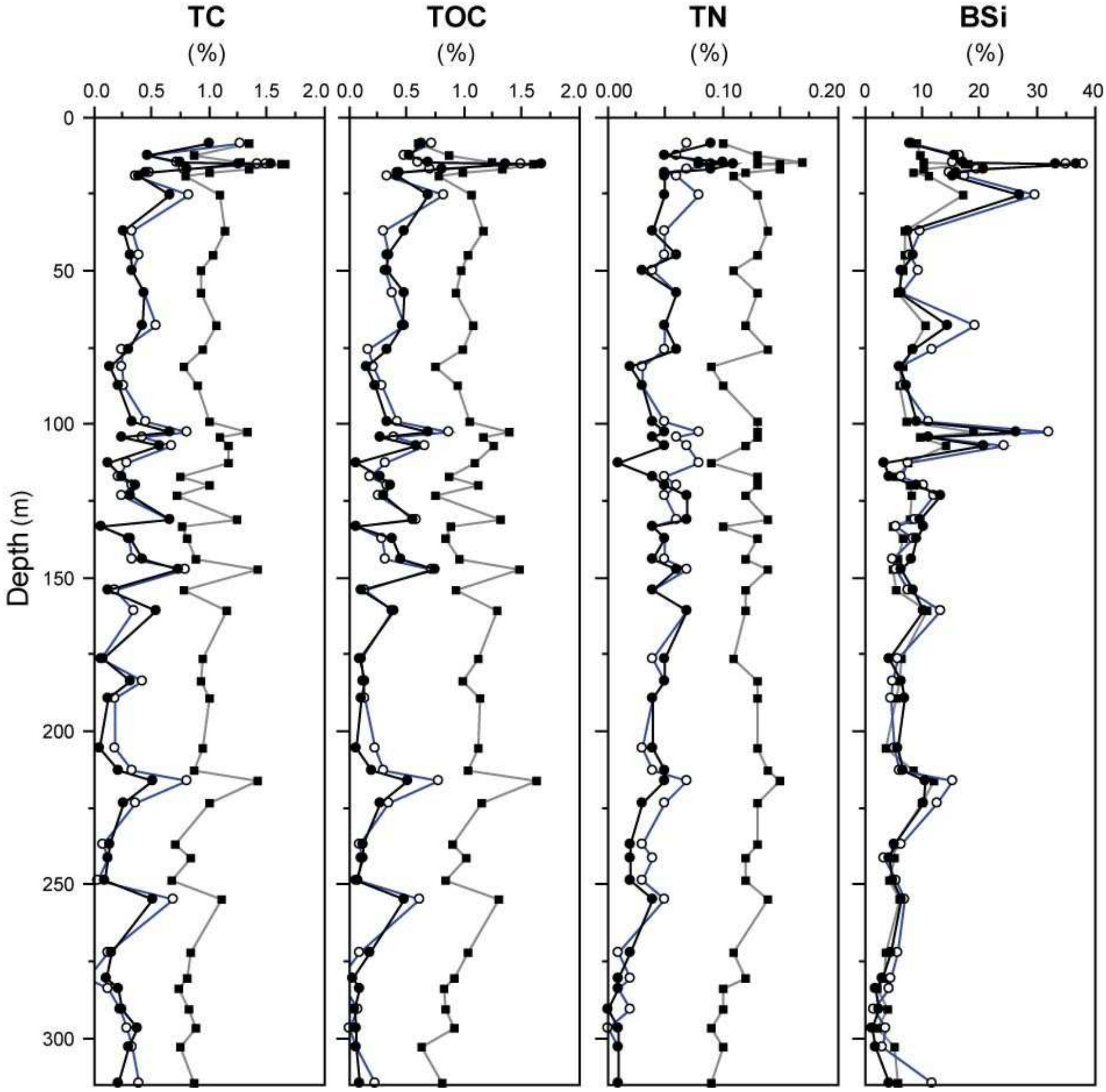

Figure 4.8 Down-core plot of biogeochemical properties of the samples from the validation set showing the prediction accuracy between conventionally measured (black line) and FTIRS-inferred values using models based on the entire sediment record of Lake El´gygytgyn (D1) (blue line) and core Lz1024 covering the uppermost sediments of the record (grey line).

ferences in the loadings between models derived from D1 and core Lz1024 probably indicate that the composition of the sediments older than ~300 ka differs from the composition of the uppermost 16.60 m of the sediment record of Lake El´gygytgyn. This means that the prediction of biogeochemical property concentrations of deeper sediments with calibration models for TC, TOC, and TN based on sediments of core Lz1024 is limited. This explains the results of the external validation showing low R^2 and high RMSEP for these models. On the contrary, predictions of BSi by the model from core Lz1024 seem not to be affected by the potential changes in the composition of the sediment. Hence, the BSi calibration model can be applied to sediments older than ~300 ka when inferring the general trend. However, absolute values have to be considered with care due to missing calibration for higher BSi concentrations. The TC model can be used with regard to the general trend. Values inferred by the calibration models for TOC and TN are deficient in this respect. Absolute values are considerably overestimated by the TOC and TN as well as the TC model of core Lz1024. These models can therefore hardly be applied to sediments from deeper parts of the sediment record, especially in the comparison with results of other studies.

MELLES et al. (2007) described four different units depending on the core description, the measured physical and chemical properties of core PG1351. Each of these units was interpreted as a different climate mode. A clearly positive correlation between BSi and organic matter (TOC, TN) was only found in one of these units interpreted as the peak warm mode and merely attributed to the Eemian (MIS 5.5). The other units showed anti-correlations or non-correlations between these properties. The dominance of the latter units throughout the core PG1351 is consistent with the low coefficient of determination between TC, TOC, TN and BSi in core Lz1024 (R^2 = 0.09-0.21). Since core PG1351 covers the uppermost ~13 m of the sediment record of Lake El´gygytgyn, this sediment sequence is also achieved in core Lz1024. In contrast to core Lz1024, there is a positive correlation between the mentioned proxies in the composite profile of D1 (R^2 = 0.52-0.62). This indicates an increased occurrence of sediment sections with a positive correlation between BSi and organic matter in the sediments of Lake El´gygytgyn with an age >300 ka. Further, this fact might be interpreted as a more common occurrence of Eemian-like, peak warm modes at Lake El´gygytgyn throughout the Old Pleistocene and Pliocene or a generally warmer climate, as is expected for instance for the mid-Pliocene (ca. 3.3-3.0 Ma) (DOWSETT et al. 1996; RAYMO et al. 1996; DOWSETT 2004).

4.4 Model Application to Marine Isotope Stage 11 (MIS 11)

The biogeochemical property concentrations of TC[2], TOC; TIC, TN, and BSi inferred by the developed FTIRS models of this study (see Table A.5 in the annex) were used to reconstruct the environmental and climatic changes at Lake El´gygytgyn during the MIS 11. In addition to these proxies, the core description and the magnetic susceptibility (C. GEBHARDT, unpublished data) were considered for the interpretation. Prior to the interpretation of the results, the inferred biogeochemical property concentrations for TC and TN were compared with the results of the conventional measurements in 2 cm resolution (V. WENNRICH, unpublished data) to estimate the accuracy of the inferred values (see Figure 4.9). The comparison shows that the predicted concentrations of TC considerably match with the conventionally measured values, whereas the TN values clearly differ. It is highly likely that this is due to the limitations of the FTIR-TN model demonstrated in Section 4.2.2. Furthermore, the underestimation of the TN concentrations can be explained by the missing of TN values above 0.17% and particularly by the existence of only two values above 0.11% in the calibration set. Due to these facts the TN values and consequently the TOC/TN ratios resulting from the conventional method in 2 cm resolution were used instead of the results of the FTIRS model application for the interpretation of the MIS 11. The extremely low values of the predicted TIC concentrations varying between 0 and 0.12% (average: 0.04%) indicate that the investigated sediment section is carbonate-free, since the limit of detection of the method on which the calibration model for TIC is based lies at approximately 0.05%. Negative values inferred by the FTIRS models probably can result when variations of the sediment properties and therefore variations of the spectral information of samples to which the FTIRS models are applied are not covered by the calibration set. These values are not considered in the interpretation.

On the basis of the considered proxies, it was possible to sub-divide the analyzed core section into five subsections. MELLES et al. (2007) distinguished four units of individual composition in core PG1351 reflecting different environmental conditions which were interpreted as climate modes (Unit 1-4). The subsections found in this study can be related to three of these four units.

---

[2] The TC concentrations originate from the calibration model based on the result of the element analyzer (TC_{EA}). FTIRS-inferred TC values from the model based on the results of the liquid analyzer (TC_{LA}) were not referred, due to the fact that these values are only slightly differ from the results of the other method (mean TC_{EA}: 0.75%; mean TC_{LA}: 0.80%).

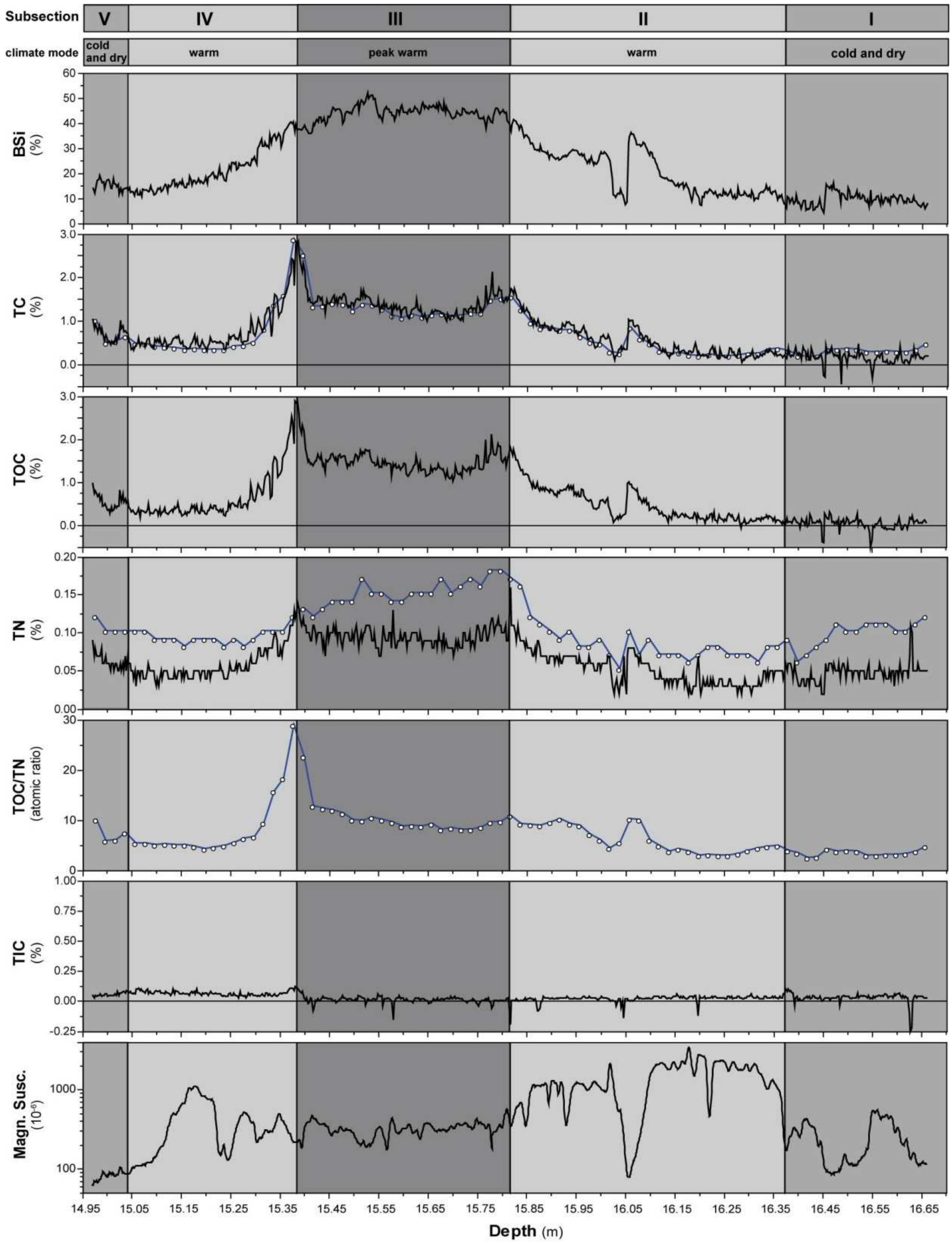

Figure 4.9 Depth plot of FTIRS-inferred biogeochemical properties (black line), conventionally measured biogeochemical properties (blue line), magnetic susceptibility, determined subsections and corresponding climate modes after MELLES et al. (2007) of the sediment section from D1 related to MIS 11.

1st Subsection

The first subsection is located at the basis of the considered core section (16.66-16.37 mblf) and is characterized by mainly layered sediments consisting of clayey silt to silt with a grey to greenish grey color. Moreover, sediment clasts and a fine sand layer with a thickness of 0.6 cm (16.45 mblf) appear in this subsection. The biogeochemical property concentrations are low and vary between 4-16% (BSi), 0-0.5% (TC), 0-0.3% (TOC), and 0.06-0.12% (TN) (see Figure 4.9). Corresponding mean concentrations are 10% for BSi, 0.2% for TC 0.1% for TOC, and 0.10% for TN. The TOC/TN ratios and the magnetic susceptibility show low values as well and alternate in the range from 2 to 4 with a mean of 3 and in the range from 85-550 × 10^{-6} with a mean of 240 × 10^{-6}, respectively. According to the classification of MELLES et al. (2007), this subsection is associated with a cold and dry climate (Unit 3). Under these conditions, a perennial ice cover on Lake El´gygytgyn is expected which inhibited a wind-generated mixing or a density-driven turnover of the water column. The latter can be excluded, since the warming of the surface water was hindered due to the ice cover. The stagnancy within the water column led then to a stratification of the lake. Despite the ice cover, the surface water of the lake apparently remained productive during this interval indicated by low but still appreciable BSi concentrations around 10%. BSi can be used as a proxy for bioproductivity, since diatom valves, which consist of biogenic silica (opal), are well preserved in the slightly acidic water of Lake El´gygytgyn. The assumption of a remarkable bioproductivity beneath the ice cover is supported by CHERAPANOVA et al. (2007) who showed that diatoms remained abundant through the cold and dry climate mode. The noticeable primary production was probably facilitated by an oxygenated habitat due to cracks in the ice cover and still favorable light conditions (BRIGHAM-GRETTE et al. 2007). HAWES et al. 2001 showed that algal and bacterial photosynthesis can proceed when less than 1% of the incident light penetrates the water column. The light penetration mainly depends on the thickness of the blanketing snow cover on the ice and not on the thickness and consistency of the ice cover itself (GORE 1997). Therefore, MELLES et al. (2007) interpreted the remained bioproductivity as a signal for a widely snow-free ice area which indicates low precipitation rates and a dry climate or strong winds blowing the snow from the ice. The occurrence of sediment clasts with a diameter of 1-2 mm is another indication for a minor or missing snow cover. The formation of these clasts could result from the agglomeration of windblown particles during their transport through the ice along vertical conduits in late summer (MELLES et al.

2007). This would be hindered by a large snow cover. As a result of the missing mixing of the water column, the bottom water became anoxic. Remaining oxygen was consumed during the decomposition of organic matter and the input of oxygenated water was interrupted. The movement of the redox boundary from within the sediments up into the water column is confirmed by low values of magnetic susceptibility. In Lake El´gygytgyn, the magnetic susceptibility depends on the conditions in the bottom water. Dissolution of magnetite, which is the dominating magnetic mineral in the sediments of the lake, occurs under reductive conditions, whereas the mineral is well preserved under oxic conditions (NOWACZYK et al. 2002; 2007). The anoxic bottom water inhibited endobenthic activity and consequently the bioturbation of the sediments which explains the preservations of distinct layers.

The TOC concentrations and the TOC/TN ratios are notably lower in the investigated core section than described by MELLES et al. (2007) for the cold and dry climate mode. MELLES et al. (2007) explain the high TOC/TN ratios by in-lake processes like nitrogen limitation in the surface water (HECKY et al. 1993) due to relatively high primary production and limited nitrogen supply as a result of the lake stratification. These processes causing higher ratios can probably be excluded, since the TOC/TN ratios are well below 10 for the considered subsection. The low values indicate an origin of the organic matter from water-column production. The TOC/TN ratio can be used as proxy for the plant source of organic matter to the lakes. It depends on the presence or absence of cellulose in the plants. Non vascular aquatic plants have low TOC/TN ratios, typically between 4 and 10, while vascular land plants containing cellulose have ratios of 20 or greater (MEYERS and ISHIWATARI 1993). However, in-lake processes can lead to misinterpretations of this proxy. The low TOC values point to a very low primary production beneath the ice coverage, especially since the anoxic conditions at the lake bottom would enhance the preservation of organic matter. This is in contradiction with the BSi concentrations indicating an appreciable bioproductivity in the surface water.

2nd Subsection

The second subsection (16.37-15.82 mblf) consists of homogenous to weakly stratified sediments of silt size with a grey to dark grey color. Furthermore, a fine sand layer with a thickness of 0.4 cm (16.20 mblf) and a turbidity layer with a graded stratification from medium fine sand to silt (16.05-16.02 mblf) are situated within the subsection. All biogeochemical property concentrations are relatively constant within the first half of the interval. They generally increase within the second half and show a small local maximum between 16.10 and 16.05 mblf (see Figure 4.9). The values increase from 8 up to 40% for BSi, from 0.2 up to 1.8% for TC, from 0.1 up to 1.8% for TOC, and from 0.06 up to 0.17% for TN. The TOC/TN ratios also rise from 3 up to 11, whereas the magnetic susceptibility remains almost continuous at a high level (average of 1300×10^{-6}). Values of the local maximum go up to 36% (BSi), 1.0% (TC), 1.0 % (TOC), 0.10% (TN), and 10 (TOC/TN), while the magnetic susceptibility decreases down to 80×10^{-6}. The turbidity layer causes a clear decrease of all proxies, except for the magnetic susceptibility. According to the classification of MELLES et al. (2007), the subsection is related to the warm climate mode (Unit 1). The conditions of this mode are comparable to the modern conditions at Lake El´gygytgyn. Mixing of the water column occurs in summer after the break-up of the semi-permanent ice cover causing an enrichment of nutrients in the surface water. This and the availability of light during the open water season enhanced the primary production in the photic zone, which is reflected by moderate BSi concentrations at the beginning of the subsection. Another result of the turnover of the water column was the ventilation and consequently the oxygenation of the bottom water. The presence of oxygen at the lake bottom is supported by high magnetic susceptibilities resulting from the preservation of magnetite under oxic conditions. Moreover, the decomposition of organic matter was enhanced by the availability of O_2 at the lake bottom shown by the low concentrations of TOC and TN in the first half of the subsection. These assumptions are sustained by the prevalent missing of stratification in the sediment which probably results from bioturbation. The activity of deep benthic organism was enabled by the availability of O_2 and organic matter from phytoplankton acting as a food source at the lake bottom. In the second half of the subsection, the biogeochemical property concentrations increase until the local maximum. This indicates a change of the climatic and/or environmental conditions at Lake El´gygytgyn enabling an enhanced primary production. Potential factors for heightened bioproductivity can for instance be an increased supply of nutrients and organic matter from the catchment, higher temperatures during the summer or a general warmer climate causing a longer open water season. The strong and rapid decline of the biogeochemical property concentrations after the local maximum is caused by a turbidity layer. Turbidites in Lake El´gygytgyn are supposed to be non-erosive or micro-erosive (JUSCHUS et al.

2009), and therefore the disturbance of the climate record is expected to be minor. Independent from the appearance of the turbidity layer, the biogeochemistry values decrease after the local maximum which points to a temporary aggravation of the conditions for bioproductivity. Afterwards, the biogeochemical property concentrations continuously increase to the maximum values of this subsection. The assumption of changes of the climatic and/or environmental conditions is supported by the TOC/TN ratios. Low ratios around 4 at the beginning of the subsection indicate a rather low supply from the catchment, whereas rising ratios up to 11 in the second half point to an increased contribution of vascular land plants to the composition of the organic matter in the lake. This suggests an increasing growth of vegetation in the catchment of Lake El´gygytgyn. The temporary aggravation of the conditions for bioproductivity is also observable in the TOC/TN ratios. Decreased values down to 4 after the local maximum can be a sign for a rather low input of organic matter from the catchment.

The significant minimum of the magnetic susceptibility with values below 100×10^{-6} around the local maximum suggest the presence of anoxic conditions, which caused dissolution of magnetite, at the lake bottom during the deposition of these sediments. However, the homogenous sediment as probable result of bioturbation by endobenthic organism, who require oxygen, and no appreciably increased concentration of organic matter due to enhanced preservation under reductive conditions are contradictory to this assumption. Furthermore, the decline is too large to simply be a result of dilution of the lithogenic fraction by biogenic input.

3rd Subsection

The third subsection (15.82-15.39 mblf) is characterized by olive grey sediments of clayey silt type with a distinctive lamination. The biogeochemical property concentrations are constantly high with average concentrations of 44% for BSi (variation: 36-52%), 1.4% for TC (variation: 1.0-2.8%), 1.5% for TOC (variation: 1.0-2.9%), as well as 0.15% for TN (variation: 0.12-0.18%) (see Figure 4.9). Furthermore, the TOC/TN ratios vary between 8 and 10 and increase considerably up to 22 at the end of the subsection, while the magnetic susceptibility is relatively constant at between 180 and 570×10^{-6}. The subsection is attributed to the peak warm climate mode (Unit 2) according to the classification of MELLES et al. (2007). This unit represents the warmest average climate conditions known from the record of PG1351 and is associated with full degradation of the lake ice cover in all years and more mixing of the water column compared to unit 1. As a result of these conditions and the favorable light penetration into the surface water, extensive plankton blooms were enabled and consequently the primary production was considerably higher. The high bioproductivity is consistent with high average BSi concentration of the subsection (44%). The TOC and TN concentrations are comparatively low, which is probably a consequence of the decomposition of the organic matter in the well oxygenated bottom water. Nevertheless, the concentrations are elevated compared to the previous subsection. This indicates that the input more clearly exceeded the degradation of organic matter leading to an incomplete decomposition. In addition to the increased input, the accompanying upward movement of the redox boundary in the sediment column probably enhanced the preservation of organic matter. Higher TOC and TN concentrations at the beginning of the subsection can be related to the occurrence of organic layers. However, the significantly higher TOC values at the end of the subsection cannot be connected to changes in the sediment composition visible with the naked eye. The TOC/TN ratios between 8 and 10 suggest a mixture of organic matter from non-vascular aquatic plants and vascular land plants, with a dominance of aquatic production. The strongly elevated ratios (up to 22) at the end of the subsection point to an increasing and finally dominating supply of organic matter from the catchment. A change in the climate and/or environment causing less favorable conditions for primary production, which is indicated by decreasing BSi concentrations, might explain this trend. Less favorable conditions would have led to a reduced aquatic primary production. The supply of organic matter from the catchment could have temporarily been constant or even enhanced due to the decline of the vegetation cover and the subsequent erosion of organic matter accumulated in the soil during the peak warm conditions into the lake. Since the duration of the MIS 11 interglacial is supposed to be about twice as long as a typical interglacial (RAYNAUD et al. 2005; PROKOPENKO et al. 2010), a high amount of organic matter could have been stored in the soils of the vicinity of Lake El´gygytgyn. A formation of organic rich soils or even peat is supposable. The increased mobilization of organic matter from the catchment as consequence of the vegetation decline might also explain the appreciably increased TOC content at the end of the subsection.

The distinctive lamination of the subsection is contradictory to the assumed well oxygenated bottom water due to the mixing of the water column. Oxic conditions would enable the activity of endobenthic organism causing bioturbation. Furthermore, the moderate magnetic susceptibility values between 180 and 570 × 10^{-6} are an indication for oxic rather than anoxic conditions, since the values are most likely a result of dilution of the lithogenic fraction by the high biogenic input and not a consequence of magnetite dissolution under reductive conditions. The identification of the origin of the lamination requires further investigations, e.g. a detailed analysis of the structure, grain-size and composition of the stratification.

4th Subsection

The fourth subsection (15.39-15.04 mblf) consists of massive to weakly stratified sediments of clayey silt to silt type with a gray to grayish brown color. All biogeochemical property concentrations decrease in the first half of the subsection and remain relatively constant in the second half. The values decrease from 41 to 11% for BSi, from 2.8 to 0.8% for TC, from 2.9 to 0.3% for TOC, and from 0.12 to 0.08% for TN (see Figure 4.9). Moreover, the TOC/TN ratio shows a comparable pattern with a decline from 29 to 4, whereas the magnetic susceptibility strongly varies between 90 and 1110 × 10^{-6}. The subsection is associated with the warm climate mode (Unit 1) according to the classification of MELLES et al. (2007) and is analogue to the second subsection, but shows an opposing trend. A successive aggravation of the conditions for primary production is indicated by the decline of the biogeochemistry property concentrations and the TOC/TN ratios at the beginning of the subsection. Decreasing values of BSi, TOC and TN suggest a reduced bioproductivity and the falling TOC/TN ratios from above 20 to 4 point to a decreasing input of organic matter from the catchment and a dominance of aquatic primary production. The latter is can be a consequence of a reduced vegetation cover around the El´gygytgyn Crater. The magnetic susceptibility values between 130 and 520 × 10^{-6} in the first half of the subsection cannot fully be explained by the dilution of the lithogenic fraction by biogenic input. Hence, anoxic bottom waters causing magnetite dissolution might, at least temporarily, be existent due to the enhanced input of organic matter at the beginning of the subsection. The second half of the subsection is characterized by more stable conditions comparable to the first half of the second subsection. After the break-up of the semi-permanent ice cover in summer, the turnover of the water column causing a ventilation of the bottom water and nutrient enrichment in the surface water and the enhanced light availability during the open water season enable an appreciable primary production. However, it is significantly lower compared to the bioproductivity during the subsection associated with the peak warm mode. The magnetic susceptibility values above 1000 × 10^{-6} suggest increased magnetite preservation due to oxic conditions at the lake bottom. This is supported by the missing of stratification in the sediment indicating the activity of endobenthic organism.

5th Subsection

The fifth subsection (15.04-14.97 mblf) is characterized by mainly stratified sediments of clayey silt type with a gray to greenish gray color and contains sediment clasts. The biogeochemical concentrations slightly increase up to 19% for BSi, up to 1.0% for TC and TOC, and up to 0.12% for TN throughout the subsection (see Figure 4.9). Furthermore, the TOC/TN ratios increase from 6 to 10, while the magnetic susceptibility is constantly below 100 × 10^{-6}. According to the classification of MELLES et al. (2007), the subsection is, like the first subsection, related to the cold and dry climate mode (Unit 3). The colder summer temperatures probably led to a perennial ice cover and consequently to a stratified water column due to inhibited turnover of the water column. The bioproductivity in the surface water remained relatively high despite the ice cover. This was enabled by an oxygenated habitat due to cracks in the ice cover and still favorable light conditions. Slightly increasing BSi values even suggest a higher primary production compared to the second half of the previous subsection. The light penetration into the surface water was probably enabled by a dry climate with low precipitation rates or strong winds causing minor snow cover on the ice. Moreover, the occurrence of sediment clasts in the subsection confirms the assumption of a widely snow-free ice cover. Sediment clasts form by agglomeration of windblown particles during their transport through the ice along vertical conduits in late summer (MELLES et al. 2007). This would be inhibited by a larger snow blanket. The establishment of anoxic bottom waters as a consequence of the lake stratification probably enhanced the preservation of organic matter which is reflected by the increased TOC and TN concentrations. Low magnetic susceptibilities due to reductive magnetite dissolution and the preservation of stratification in the sediment indicating the absence of endobenthic activity support the existence of anoxic conditions at the lake bottom. As MELLES et al. (2007) assumed, the increasing TOC/TN ratios are probably a result of in-lake processes rather than an indication for enhanced supply of organic matter from vascular land plants. Input from the catchment is unlikely in view of the cold climate. An explanation might be nitrogen limitation in the surface water as a consequence of the relatively large export production and the presumably limited nitrogen supply due to the ice cover and stratification of the water column.

Driving Factors of Changes in the Sediment Composition

The PCA of the samples from the investigated core section shows the changes in the sediment composition solely based on the FTIR-spectral information. The loadings of the first principle component (PC 1) explaining 74% of the spectral variations are strongly similar to the loadings of the FTIRS calibration model for BSi (see Figure 4.10). Furthermore, variations in a depth plot of the PC 1 scores are mainly consistent with variations in the BSi concentrations (see Figure 4.11). These analogies demonstrate that changes in the sediment composition are basically ascribed to biogenic silica whose FTIRS-inferred content is varies between 4 and 52% throughout the analyzed core section. Due to the good preservation of diatom valves consisting of biogenic silica in the slightly acidic water of Lake El´gygytgyn, BSi can be used as proxy for bioproductivity (MELLES et al. 2007; NOWACZYK et al. 2007). Apart from temperature and nutrient supply, bioproductivity basically depends on the availability of light. The intensity of the sunlight reaching the surface of the earth varied in the geological past due to insola-

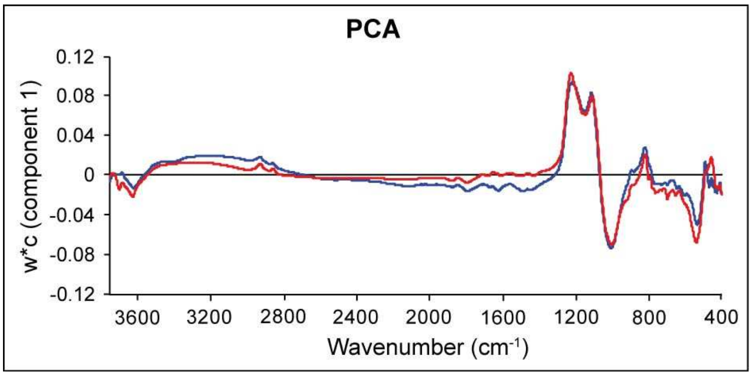

Figure 4.10 Loading plots of the first principle component (PC) from a PCA of the FTIR spectra from the sediments related to MIS 11 (red line) and the first component of the PLSR model for BSi (blue line) showing the contribution of each wavenumber to the PC/PLSR model. Positive values indicate wavenumbers positively correlated to the property of interest and negative values indicate wavenumbers negatively correlated to the property of interest. Loadings are expressed by weight vectors (w*c) of the PC/PLSR model (component 1) (y-axis) and the corresponding wavelength range (x-axis).

tion changes. Variations of the insolation are dependent on quasi-cyclic changes in the obliquity (41 kyr) and the precession (18 and 23 kyr) of the earth´s axis of rotation, and variations in the eccentricity (100 and 400 kyr) of the earth´s orbit around the sun (NOWACZYK et al. 2007).

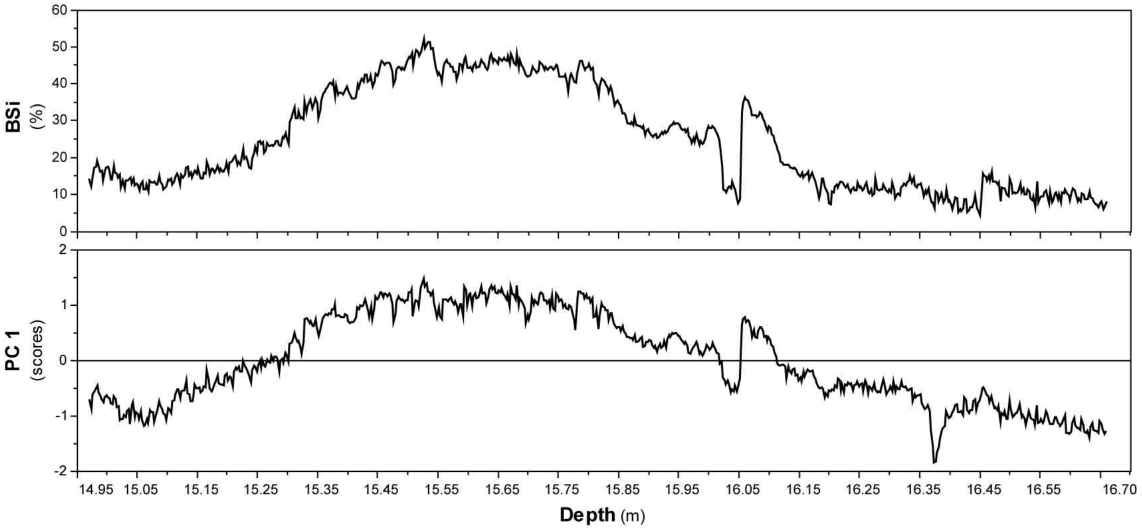

Figure 4.11 Depth plot of the FTIRS-inferred BSi concentrations and the scores of the first principle component (PC 1) of a PCA of the core section related to MIS 11 showing strong similarities.

The biogenic silica record of Lake Baikal (PROKOPENKO et al. 2006) and the temperature reconstruction from the EPICA (European Project for Ice Coring in Antarctica) Dome C ice core (JOUZEL et al. 2007) show a very similar pattern to the inferred BSi record of the core section from Lake El´gygytgyn analyzed in this study (see Figure 4.12). This facilitates an approximate estimation of the chronological position of the considered core section. With the help of this information, it is possible to include the insolation in the interpretation of the variations of the biogeochemical property concentrations (see Firgure 4.12). The precession-driven maxima of total insolation per year (BERGER and LOUTRE 1991) occurred at the beginning of both the small and the prolonged maxima of the BSi concentration record. This corresponds well with the assumption for the insolation-tuned age model of core PG1351; that insolation maxima are situated at the beginning of warm stages (NOWACZYK et al. 2007). The BSi concentrations during MIS 11 clearly exceeded the concentrations during the warm stages (MIS 1-7) known from core PG1351. However, the insolation maxima of these warm stages were similar or even higher than the maximum of MIS 11. Thus, the productivity is apparently not only controlled by the intensity of insolation. MELLES et al. (2007) suggested that the supply of nutrients and organic matter from the catchment is the major driving factor for bioproductivity in Lake El´gygytgyn during warm stages. This assumption is supported by the findings of this study showing higher concentrations of TOC and TN in MIS 11 compared to the warm stages archived in the sediments of core PG1351. The higher values probably indicate an enhanced input from the catchment during MIS 11. The amount of this supply strongly depends on the structure of the terrestrial vegetation cover (MELLES et al. 2007).

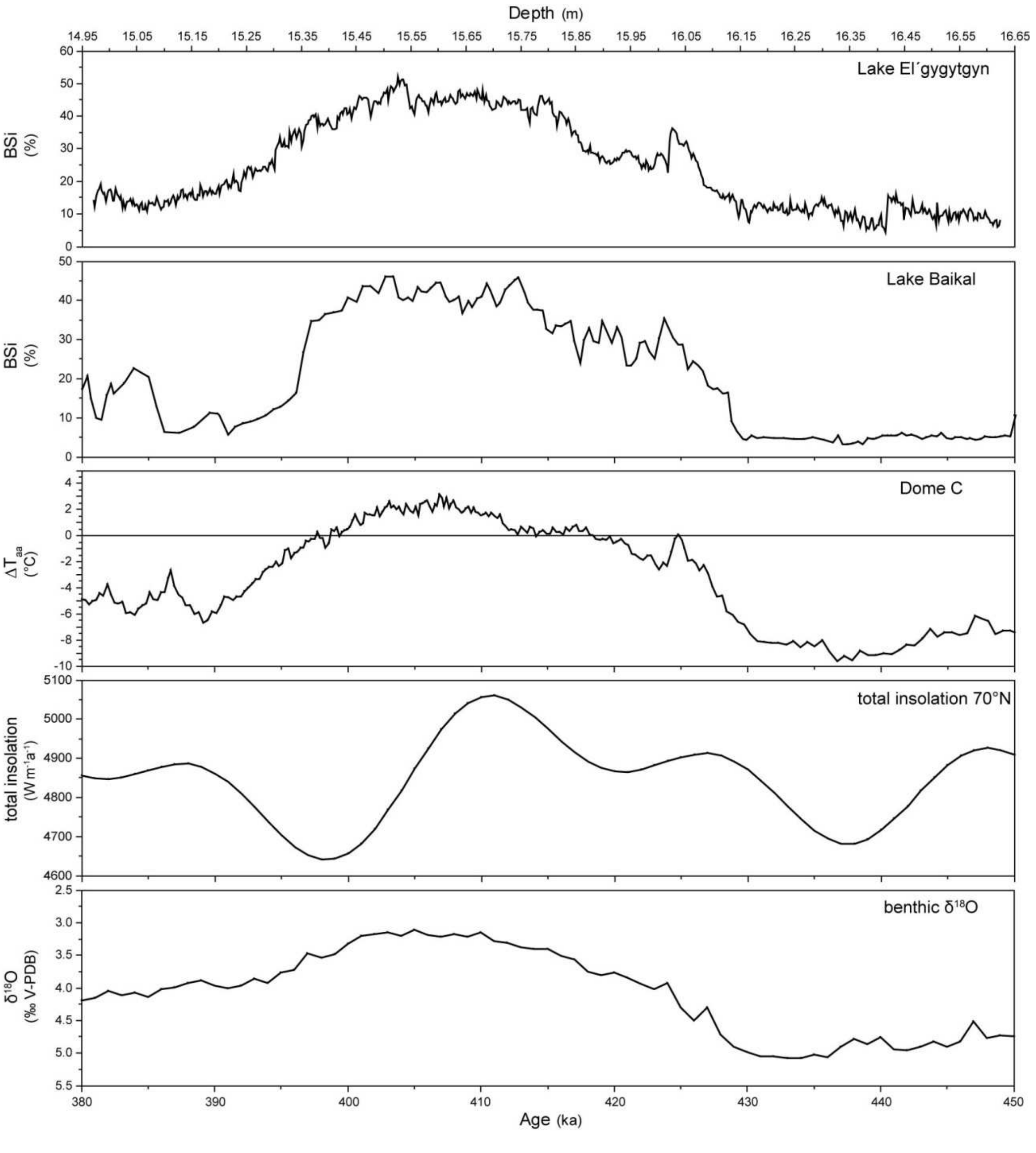

Figure 4.12 Correlation between the biogenic silica record of Lake El´gygytgyn (turbidite excluded)versus depth and the biogenic silica record of Lake Baikal (PROKOPENKO et al. 2006), the temperature reconstruction from EPICA Dome C ice core (temperature anomaly relative to the mean of the last 1000 yr (ΔT_{aa})) (JOUZEL et al. 2007), the total insolation per year at 70°N (BERGER and LOUTRE 1991) and the global benthic δ18O stacked record (LISIECKI and RAYMO 2005) versus age of the interval related to MIS 11.

Duration of MIS 11

The strong similarity between the biogenic silica record of Lake El´gygytgyn and the record of Lake Baikal (see Figure 4.12) suggests a duration of the MIS 11 in the Siberian Arctic comparable to the duration of about 30 kyr known from continental interior Asia (PROKOPENKO et al. 2010). Prolonged stable interglacial conditions are indicated by sustained high accumulation rates of BSi and organic matter. The extraordinary long duration of MIS 11 is consistent with results of other study sites in Antarctica (RAYNAUD et al. 2005) and NW Africa (HELMKE et al. 2008). An explanation for this long duration might be the low amplitude of insolation variations and the long lasting high CO_2 concentrations during MIS 11. Under these conditions, the ice sheets are prevented from growing and prolonged stable interglacial conditions are possible (LOUTRE and BERGER 2003; RAYNAUD et al. 2005). Furthermore, the interval of MIS 11 coincides well with the maximum of the same interval from the global benthic δ18O stacked record by LISIECKI and RAYMO (2005) (see Figure 4.12).

4.5 Potential Diagenetic Changes in the Sediment Record

It was possible to develop a calibration model that infers the burial depth of a sample by means of its spectral information. The corresponding FTIRS calibration model shows a significant correlation between the IR-inferred depth and the depth of the sample conventionally determined during the drilling process. An R_{cv}^2 of 0.88, an RMSECV of 24.4 m (7.8% of the gradient), an R^2 of 0.86 (see Figure 4.13) and an RMSEP of 35.2 m (11.5% of the gradient) result from the internal and external validation, respectively. Therefore, it seems that IR-spectra of the sediment samples might contain information related to their burial depth. The loading plot of the corresponding model shows strong similarities to the loading plot of the calibration model developed for BSi, but has an inverse trend (see Figure 4.13). This can be explained by the general trend of decreasing BSi concentrations with increasing depth within the sediment record. An R^2 of 0.45 highlights the moderate correlation between both parameters. However, this correlation explains only partly the possibility to determine the sample depth on the basis of the spectral information, since different FTIRS-inferred burial depths result from samples of equal BSi content.

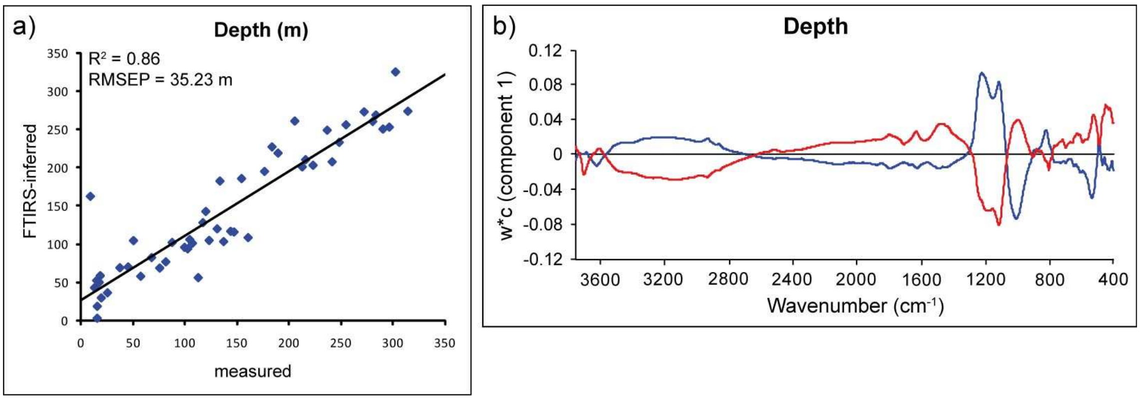

Figure 4.13 a) Scatter plot of conventionally measured (x-axis) versus FTIRS-inferred depth (y-axis) **b)** Loading plots of the FTIRS models for the burial depth (red line) and BSi (blue line) showing the contribution of each wavenumber to the PLSR model. Positive values indicate wavenumbers positively correlated to the property of interest and negative values indicate wavenumbers negatively correlated to the property of interest. Loadings are expressed by weight vectors (w*c) of the PLSR model (component 1) (y-axis) and the corresponding wavelength range (x-axis).

The spectral region between 2,600 and 3,750 cm^{-1} might be particularly relevant for the explanation of the depth-related information in the FTIR spectra. Absorption in this region is mostly related to molecular vibrations of hydroxyl groups (MOENKE 1974a; KELLNER et al. 2004) which are contained in organic matter and several minerals such as clay minerals or biogenic silica. On the one hand, the importance of this region is indicated by its higher loading values compared to the loadings of BSi model. On the other hand, single FTIR spectra show decreasing absorbance in the region with increasing burial depth (see Figure 4.14). However, single spectra of the record of Lake El´gygytgyn have to be considered with reservation, since their exact composition is unknown and the proportion of components containing hydroxyl groups can strongly vary. Further, it was possible to develop a calibration model for the depth only based on the spectral region between 2,600 and 3,750 cm^{-1}. The model has an R_{cv}^2 of 0.87, an RMSECV of 29.0 m (9.3% of the gradient), an R^2 of 0.93, and an RMSEP of 26.4 m (8.6% of the gradient). Hence, the results of the internal and external validation of this model only slightly differ from the results of the model based on the entire spectrum. The negative correlation of this range might indicate a dehydration/dehydroxylation of certain mineral phases with increasing burial depth. SCHMIDT et al. (2001) and RICKERT et al. (2002) suggested a loss of hydroxyl water during the silica maturation in the surface sediments due to internal condensation reactions. This process might be continued with increasing sediment maturation. Another potential source of OH release is the transformation of opal-A to opal-CT. This process normally occurs at temperatures around 50°C (Murata et al. 1977; Hein et al. 1978) and is probably unlikely in the sediment body of Lake El´gygytgyn whose maximum temperature probably not exceeds 20°C (El´gygytgyn Science Party, unpublished data). However, studies of Matheney and Knauth (1993) have suggested that opal-CT can form at temperatures much lower than previously assumed (17-21°C). Furthermore, Botz and Bohrmann (1991) have reported that opal-CT is forming in Antarctic deep-sea sediments at 0-4°C.

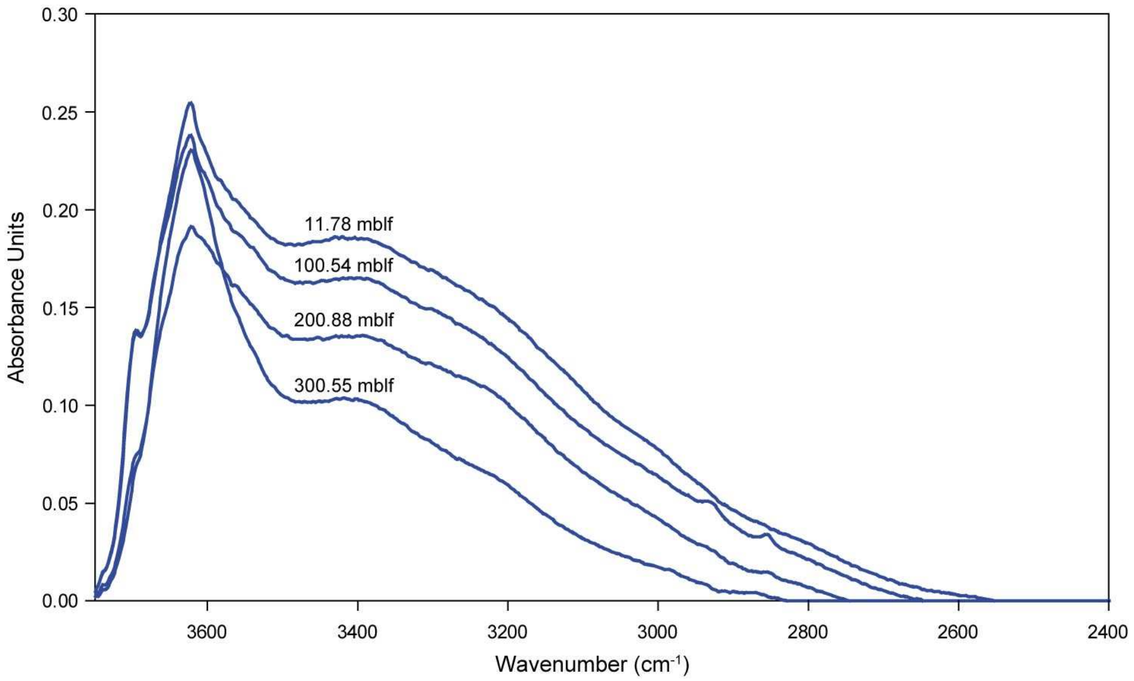

Figure 4.14 FTIR spectra of sediment samples from Lake El´gygytgyn with different burial depths (11.78, 100.54, 200.88, 300.55 mblf) in the wavenumber range 2,400-3,750 cm^{-1} indicating dehydroxylation/dehydration processes with increasing burial depth.

FTIR spectroscopy can be used to detect if the transformation of opal-A to opal-CT and/or internal condensation reactions occur in the sediment record of Lake El´gygytgyn. Rice et al. (1995) showed that the absorption peak around 470 cm^{-1} shifts towards higher wavenumbers as opal-A is converted to opal-CT. The peak at around 470 cm^{-1} is attributed to Si-O-Si bending vibrations in non-crystalline opal (Moenke 1974b; Gendron-Badou et al 2003). Opal-CT is a paracrystalline mineral formed of short-range ordering domains that mimic the arrangement of cristobalite and tridymite in a matrix of disordered opal (Rodgers et al. 2004). Si-O-Si bending vibrations in cristobalite are situated at around 490 cm^{-1} (Moenke 1974b). Schmidt et al. (2001) suggested that within surface sediments the structure and composition of biogenic silica changes due to in-situ condensation of Si-OH groups and formation of Si-O-Si linkages.

The ratios between integrated absorptions at 800 $\mathrm{cm^{-1}}$ and 950 $\mathrm{cm^{-1}}$ were used as parameter for the maturation of biogenic silica. Inter-tetrahedral Si-O-Si bending vibration modes cause absorption of IR radiation at around 800 $\mathrm{cm^{-1}}$, while absorptions at around 950 $\mathrm{cm^{-1}}$ can be related to Si-OH molecular vibrations (MOENKE 1974b; GENDRON-BADOU et al 2003). FTIR spectra of a diatom sample (opal-A) and a porcelanite (opal-CT) demonstrate the dehydration/dehydroxylation of biogenic silica during the transformation of opal-A to opal-CT (see Figure 4.15). The shift of the absorption band around 470 $\mathrm{cm^{-1}}$ to higher wavenumbers, as well as the decrease of the absorption band at around 950 $\mathrm{cm^{-1}}$ connected to Si-OH molecular vibrations is observable. Furthermore, reduced absorbance in the spectral region between 2,600 and 3,750 cm indicating a release of hydroxyl groups support the importance of this spectral region for the explanation of the depth-related information in the FTIR spectra. FTIR spectra of pure diatom samples from deeper parts of the sediment record of Lake El´gygytgyn can probably shed light on the question if dehydration/dehydroxylation processes occur in the sediment record and if these processes are connected with biogenic silica.

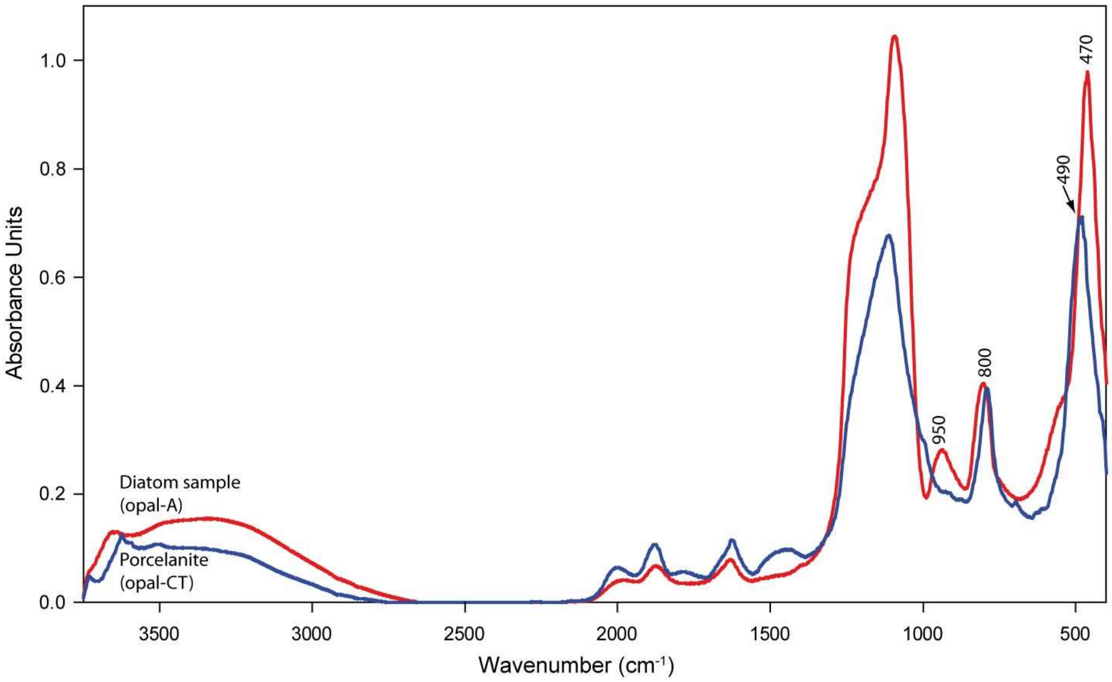

Figure 4.15 FTIR spectra of a diatom sample (opal-A) from Lake El´gygytgyn (red line) and a porcelanite from Morocco (Meskala Formation) (blue line) showing the spectral changes during the transformation of opal-A to opal-CT.

4.6 Carbonates in the Sediment Record

A first evaluation of the FTIR spectra has shown that several samples of the sediment record of Lake El´gygytgyn contain absorption peaks related to carbonate minerals. Consequently, conventional measurement and subsequent a FTIR model were applied to determine the carbonate content of the samples. By means of FTIRS, it was also possible to differentiate between two carbonate mineral phases. Calcite ($Ca[CO_3]$), on the one hand, shows distinct absorption peaks at 712, 876, 1,435, 1,812, and 2,545 cm^{-1} and siderite ($Fe[CO_3]$), on the other hand, has specific peaks at 737, 866, 1,422, and 1,818 cm^{-1} (HUANG and KERR 1960). Due to the low concentrations of carbonates in the sediment samples (see Figure 4.16 and Table A.6 in the annex), a clear determination of siderite was only possible for one sample (8.79 mblf), whereas calcite was determined in several samples in the lowermost past of the sediment record.

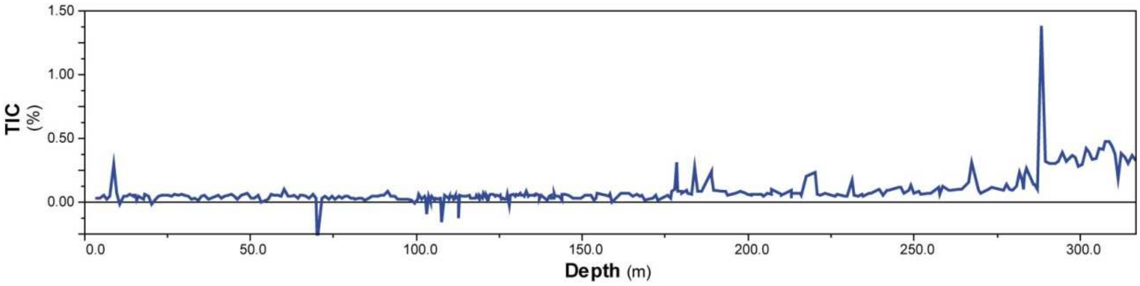

Figure 4.16 Depth plot of the FTIRS-inferred TIC concentrations of D1.

The occurrence of calcite is confirmed by XRD measurements (see Figure 4.17), while siderite was also detected with the help of thermomagnetic measurements (P. MINYUK, pers. commun. 2010). The origin of the carbonates in the sediments of Lake El´gygytgyn is unknown and further investigations are required. Carbonate precipitation in the water column is unlikely under present lake conditions due to the slightly acidic pH (CREMER and WAGNER 2003). The increased occurrence of carbonates at the basis of the sediment body might indicate a formation of calcite due to hydrothermal activity induced by the meteorite impact (OSINSKI et al. 2001, 2005). Calcite veins found in the underlying impact breccia (U.RASCHKE, pers. commun. 2010) may also have been formed in this context.

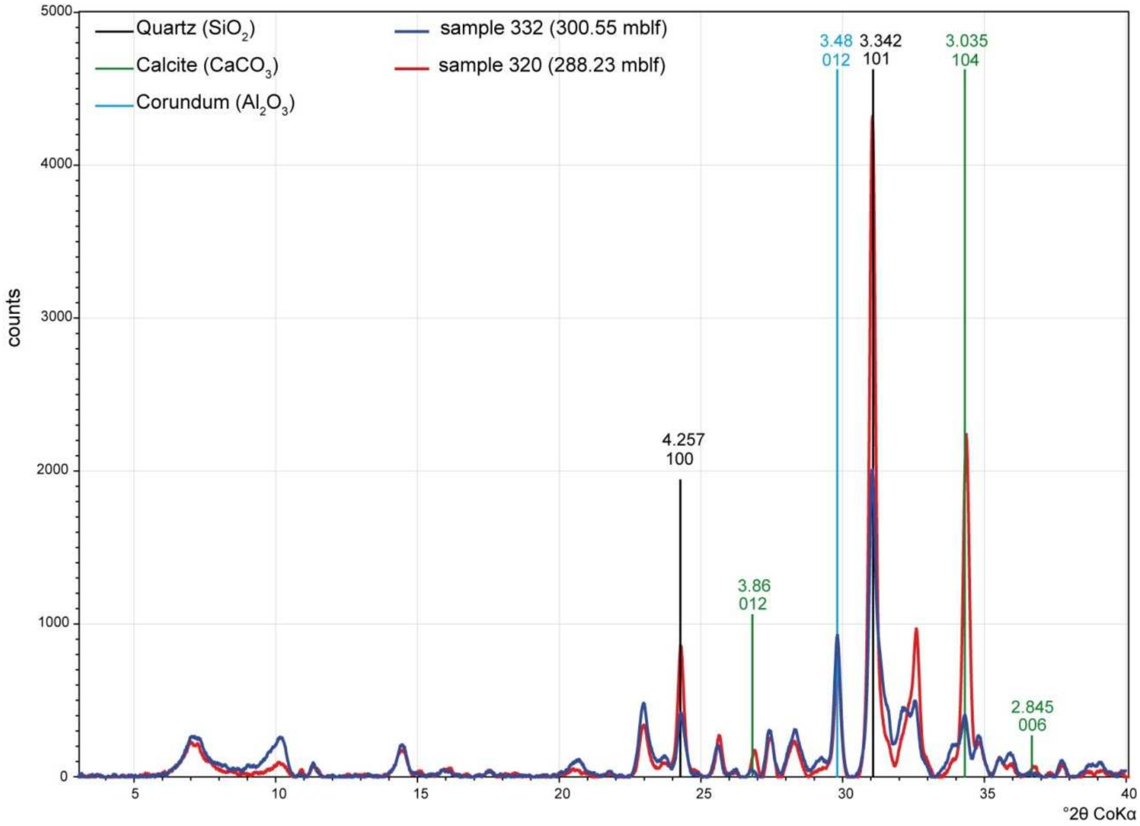

Figure 4.17 Diffractogram of two samples from the sediment record of Lake El´gygytgyn containing calcite.

5 Conclusions and Outlook

This study shows that it is possible to develop robust FTIRS calibration models for the quantitative assessments of biogeochemical properties in the sediment record of Lake El´gygytgyn despite its length (~315 m) and age (up to 3.6 Ma). Wavenumbers used by the models are consistent with known molecular vibrations of several organic and minerogenic compounds. The statistical performance was good for calibration models of TC, TOC, TIC, and BSi, and moderate for the calibration model of TN relating FTIR spectral information and conventional measurements. Therefore, these models can be applied to the sediments of Lake El´gygytgyn in high-resolution to assess quantitatively the component of interest in a rapid and cost-efficient way. An internal calibration including samples from the entire sediment record is probably essential to obtain reliable results from a sediment sequence of several hundred meters. Results inferred by applying calibration models only based on the uppermost part of the sedimentary record to sediments from deeper parts of the record were unreliable for TC, TOC and TN. It is likely that the sediment composition of the deeper parts of the sediment record differs from the composition of the uppermost sediments. Therefore, models only derived from this part cannot predict accurately biogeochemical property concentrations in the entire record. However, reasonable results could be obtained for BSi. This proxy seems to be less affected by changes in the sediment composition.

The results of the application of the developed FTIRS models to sediments of MIS 11 suggest that this period was a particularly pronounced interglacial showing a very high bioproductivity compared to younger interglacials at Lake El´gygytgyn. The bioproductivity within the lake is probably dependent on the input of nutrients and organic matter from the catchment rather than insolation forcing. The duration of the MIS 11 in the Siberian Arctic is presumably comparable to its prolonged duration in continental interior Asia where it lasted for approximately 30 kyr (PROKOPENKO et al. 2010). Moreover, the recorded FTIR spectra indicate diagenesis induced changes of sediment composition. However, further investigations are required for the confirmation of these changes. Two carbonate phases, calcite and siderite, could also be differentiated in the sediments of Lake El´gygytgyn by means of FTIRS, but their origin remains unclear.

More research has to be done to use the full potential of FTIRS. Since the method provides information about both organic and minerogenic compounds, it is probably possible to determine and quantify further components in sediments. The results of this study and the results of Vogel et al. (2008) and Rosén et al. (2010) show that FTIRS has the potential to become a useful tool in paleoclimate research.

6 References

Andrade JM, Garcia MV, Lopez-Mahia P, Prada D (1997) A review of the main factors influencing the FT-IR-PLS abilities exemplified with petrochemical qualimetric applications. Talanta 44:2167-2184.

Antti H (1999) Multivariate Characterization of Wood Related Materials. Dissertation. Umeå University, Umeå, Sweden.

Asikainen CA, Francus P, Brigham-Grette J (2007) Sedimentology, clay mineralogy and grain-size as indicators of 65 ka of climate change from El´gygytgyn Crater Lake, Northeastern Siberia. Journal of Paleolimnology 37:105-122.

Belzile N, Joly HA, Li H (1997) Characterization of humic substances extracted from Canadian lake sediments. Canadian Journal of Chemistry 75:14-27.

Berger A, Loutre MF (1991) Insolation values for the climate of the last 10 million years. Quaternary Science Reviews 10:297-317.

Bertaux J, Ledru MP, Soubiès F, Sondag F (1996) The use of quantitative mineralogy linked to palynological studies in paleoenvironmental reconstruction: the case study of the “Lagoa Campestre” lake, salitre, Minas Gerais, Brazil. Comptes rendus de l´Académie des scienes 323(Series II):65-71.

Bertaux J, Fröhlich F, Ildefonse P (1998) Multicomponent analysis of FTIR spectra: quantification of amorphous and crystallized mineral phases in synthetic and natural sediments. Journal of Sedimentary Research 68:440-447.

Botz R, Bohrmann G (1991) Low-temperature opal-CT precipitation in Antarctic deep-sea sediments: evidence from oxygen isotopes. Earth and Planetary Science Letters 107:612-617.

Braguglia CM, Campanella L, Petronio BM, Scerbo R (1995) Sedimentary humic acids in the continental margin of the Ross Sea (Antarctica). International Journal of Environmental Analytical Chemistry 60:61-70.

Brigham-Grette J, Melles M, Juschus O (2005) Terrace 10 m below lake level (chapter 5.3.2). In: Melles M, Minyuk P, Brigham-Grette J, Juschus O (eds.) The Expedition El´gygytgyn Lake 2003 (Siberian Arctic). Reports on Polar and Marine Research 509:108-110.

Brigham-Grette J, Melles M, Minyuk P (2007) Overview and significance of a 250 ka paleoclimate record from El´gygytgyn Crater Lake, NE Siberia. Journal of Paleolimnology 37:1-16.

Calace N, Capolei M, Lucchese M, Petronio BM (1999) The structural composition of humic compounds as indicator of organic carbon sources. Talanta 49:277-284.

Calace N, Cardellicchio N, Petronio BM, Pietrantonio M, Pietroletti M (2006) Sedimentary humic substances in the northern Adriatic sea (Mediterranean sea). Marine Environmental Research 61:40-58.

Chapman SJ, Campbell CD, Fraser AR, Puri G (2001) FTIR spectroscopy of peat in and bordering Scots pine woodland: relationship with chemical and biological properties. Soil Biology & Biochemistry 33:1193-1200.

Cherapanova MV, Snyder J, Brigham-Grette J (2007) Diatom stratigraphy of the past 250 ka from El´gygytgyn Lake sediments, northeastern Russia. Journal of Paleolimnology 37:155-162.

Cocozza C, D’Orazio V, Miano TM, Shotyk W (2003) Characterization of solid and aqueous phases of a peat bog profile using molecular fluorescence spectroscopy, ESR and FT-IR, and comparison with physical properties. Organic Geochemistry 34:49-60.

Colthup NB; Daly LH; Wiberley SE (1975) Introduction to Infrared and Raman spectroscopy. Academic Press, New York, San Francisco, London.

Conley DJ (1998) An interlaboratory comparison for the measurement of biogenic silica in sediments. Marine Chemistry 63:39-48.

Cremer H, Wagner B (2003) The diatom flora in the ultra-oligotrophic Lake El´gygytgyn, Chukotka. Polar Biology 26:105-114.

Dehnert A (2004) Rezente Sedimentation im El´gygytgyn See, NO Sibirien, abgeleitet aus der Zusammensetzung von Oberflächensedimenten [Recent sedimentation in Lake El´gygytgyn, NE Siberia, inferred from the composition of surface sediments]. Diploma Thesis. Leipzig, Germany: Institute for Geophysics and Geology, University of Leipzig.

DeMaster DJ (1981) The supply and accumulation of silica in the marine environment. Geochimica et Cosmochimica Acta 45:1715-1732.

Dowsett H (2004) Bracketing Mid-Pliocene sea surface temperature: maximum and minimum possible warming. U.S. Geological Survey Data Series, vol. 114.

Dowsett H, Barron J, Poore R (1996) Middle Pliocene sea surface temperatures: a global reconstruction. Marine Micropaleontology 27:13-25.

Farmer VC (1974) The layer silicates. In: Farmer VC (ed.) The infrared spectra of minerals. Mineralogical Society Monograph 4, Adlard & Son, Dorking, Surrey, pp 331-363.

Gebhardt AC, Niessen F, Kopsch C (2006) Central ring structure identified in one of the world´s best-preserved impact craters. Geology 34:145-148.

Geladi P, MacDougall D, Martens H (1985) Linearization and scatter-correction for near-infrared reflectance spectra of meat. Applied Spectroscopy 39:491-500.

Gendron-Badou A, Coradin T, Maquet J, Fröhlich F, Livage J (2003) Spectroscopic characterization of biogenic silica. Journal of Non-Crystalline Solids 316:331-337.

Glushkova OYu, Smirnov VN (2007) Pliocene to Holocene geomorphic evolution and paleogeography of the El´gygytgyn Lake region, NE Russia. Journal of Paleolimnology 37:37-47.

Gore DB (1997) Blanketing snow and ice; constraints on radiocarbon dating deglaciation in East Antarctica. Antarctic Science 9:336-346.

Grebmeier JM, Overland JE, Moeere SE, Farley EV, Carmack EC, Cooper LW, Frey KE, Helle JH, McLaughlin FA, McNutt SL (2006) A major ecosystem shift in the northern Bering Sea. Science 311:1461-1462

Griffiths PR, de Haseth JA (2007) Fourier Transform Infrared Spectroscopy. Wiley, New York.

Gurov EP, Koeberl C (2004) Shocked rocks and impact glasses from the El´gygytgyn impact structure, Russia. Meteoritics & Planetary Science 39:1495–1508.

Harris DC (2007) Quantitative Chemical Analysis. W.H. Freeman and Company.

Hawes I, Moorhead D, Sutherland D, Smeling J, Schwarz AM (2001) Benthic primary production in two perennially ice-covered Antarctic lakes: patterns of biomass accumulation with a model of community metabolism. Antarctic Science 13:18-27.

Hecky RE, Campbell P, Hendzel LL (1993) The stoichiometry of carbon, nitrogen, and phosphorus in particulate matter of lakes and oceans. Limnology and Oceanography 38:709-724.

Hein JR, Scholl DW, Barron JA, Jones MG, Miller J (1978) Diagenesis of late Cenozoic diatomaceous deposits and formation of the bottom simulating reflector in the southern Bering Sea. Sedimentology 25:155-181.

Helmke JP, Bauch HA, Röhl U, Kandiano ES (2008) Uniform climate development between the subtropical and subpolar Northeast Atlantic across marine isotope stage 11. Climate of the Past 4:181-190.

Herbert TD, Brian AD, Burnett C (1992) Precise major component determination in deep-sea sediments using Fourier transform infrared spectroscopy. Geochimica et Cosmochimica Acta 56:1759-1763.

Huang CK, Kerr PF (1960) Infrared study of the carbonate minerals. American Mineralogist 45:311-324.

Ispolatov VO, Tikhomirov PL, Heizler M, Cherepanova IYu (2004) New $^{40}Ar/^{39}Ar$ ages of Cretaceous continental volcanics from Central Chukotka: implications for initiation and duration of volcanism within the northern part of the Okhotsk Chukotka volcanic belt (Northeastern Eurasia). Journal of Geology 112:369-377.

Johnston S (1991) Fourier transform infrared: a constantly evolving technology. Ellis Horwood, New York, London, Toronto, Sydney, Tokyo, Singapore.

Jouzel J, Masson-Delmotte V, Cattani O, Dreyfus G, Falourd S, Hoffmann G, Minster B, Nouet J, Barnola JM, Chappellaz J, Fischer H, Gallet JC, Johnson S, Leuenberger M, Loulergue L, Luethi D, Oerter H, Parrenin F, Raisbeck G, Raynaud D, Schilt A, Schwander J, Selmo E, Souchez R, Spahni R, Stauffer B, Steffensen JP, Stenni B, Stocker TF, Tison JL, Werner M, Wolff EW (2007) Orbital and millennial Antarctic climate variability over the past 800,000 years. Science 317:793-796.

Juschus O, Wennrich V, Quart S, Minyuk P, Melles M, Gebhardt C, Niessen F (2005) New long Record Lz1024 (chapter 6.1.1). In: Melles M, Minyuk P, Brigham-Grette J, Juschus O (eds.) The Expedition El´gygytgyn Lake 2003 (Siberian Arctic). Reports on Polar and Marine Research 509:110-113.

Juschus O, Preusser F, Melles M, Radtke U (2007) Applying SAR-IRSL methodology for dating fine-grained sediments from Lake El´gygytgyn, north-eastern Siberia. Quaternary Geochronology 2:187-194.

Juschus O, Melles M, Gebhardt C, Niessen F (2009) Late Quaternary mass movement events in Lake El´gygytgyn, North-eastern Siberia. Sedimentology 56:2155-2174.

Juschus O, Pavlov M, Schwammborn G, Federov G, Melles M (subm.) Late Quaternary Lake-Level Changes of Lake El´gygytgyn, NE Siberia. Quaternary Research.

Keigwin LD (1998) Glacial-age hydrography of the far northwest Pacific Ocean. Paleoceanograhy 13:323-339.

Kelley SP, Spicer RA, Herman AB (1999) New $^{40}Ar/^{39}Ar$ dates for Cretaceous Chauna Group tephra, northeastern Russia, and their implications for the geologic history and floral evolution of the North Pacific region. Cretaceous Research 20:97-106.

Kellner R; Mermet J-M; Otto M; Valcárcel H, Widmer HM (2004) Analytical chemistry: a modern approach to analytical science. Wiley-VCH, Weinheim, Berlin, New York, Chichester, Brisbane, Singapore, Toronto.

Layer P (2000) Argon-40/argon-39 age of the El´gygytgyn impact event, Chukotk, Russia. Meteoritics & Planetary Science 35:591-599.

Lisiecki LE, Raymo ME (2005) A Plio-Pleistocene stack of 57 globally distributed benthic $\delta^{18}O$ records. Paleoceanography 20, PA1003, 17 pp. doi:10.1029/2004PA001071.

Loutre MF, Berger A (2003) Marine Isotope Stage 11 as an analogue for the present interglacial. Global and Planetary Change 36:209-217.

Lozhkin AV, Anderson PM, Matrosova TV, Minyuk PS (2007) Vegetation and climate histories of El`gygytgyn Lake, Northeast Siberia. Journal of Paleolimnology 37:135-153.

Madejová J (2003) FTIR techniques in clay mineral studies. Vibrational Spectroscopy 31:1-10.

Martens H; Næs T (1989) Multivariate Calibration. John Wiley & Sons, Chichester, New York, Brisbane, Toronto, Singapore.

Matheney RK, Knauth LP (1993) New isotopic temperature estimates for early silica diagenesis in bedded cherts. Geology 21:519-522.

Mecozzi M, Pietrantonio E, Amici M, Romanelli G (2001) Determination of carbonate in marine solid samples by FTIR-ATR spectroscopy. Analyst 126:144-146.

Mecozzi M, Pietrantonio E (2006) Carbohydrates proteins and lipids in fulvic and humic acids of sediments and its relationships with mucilanginous aggregates in the Italian seas. Marine Chemistry 101:27-39.

Melles M, Brigham-Grette J, Glushkova OY, Minyuk PS, Nowacyk NR, Hubberten H-W (2007) Sedimentary geochemistry of core PG1351 from Lake El´gygytgyn –

a sensitive record of climate variability in the East Siberian Arctic during the past three glacial-interglacial cycles. Journal of Paleolimnology 37:89-104.

Melles M, Juschus O, Wennrich V, Brigham-Grette J, Gebhardt C (2009) The impact of mass movement events on the pelagic sediment record in Lake El´gygytgyn, NE Russia. Abstract AGU Fall Meeting 2009.

Meyers PA, Ishiwatari R (1993) Lacustrine organic geochemistry – an overview of indicators of organic matter sources and diagenesis in lake sediments. Organic Geochemistry 20:867-900.

Minyuk PS, Brigham-Grette J, Melles M, Borkhodoev VYa, Glushkova OYu (2007) Inorganic geochemistry of El´gygytgyn Lake sediments (northeastern Russia) as indicator of paleoclimatic change for the last 250 kyr. Journal of Paleolimnology 37:123-133.

Moenke HHW (1974a) Vibrational spectra and the crystal-chemical classification of minerals. In: Farmer VC (ed.) The infrared spectra of minerals. Mineralogical Society Monograph 4, Adlard & Son, Dorking, Surrey, pp 111-118.

Moenke HHW (1974b) Silica, the three-dimensional silicates, borosilicates and beryllium silicates. In: Farmer VC (ed.) The infrared spectra of minerals. Mineralogical Society Monograph 4, Adlard & Son, Dorking, Surrey, pp 365-382.

Müller PJ, Schneider J (1993) An automated leaching method for the determination of opal in sediments and particulate matter. Deep Sea Research 40:424-444.

Murata KJ, Friedman I, Gleason JD (1977) Oxygen isotope relations between diagenetic silica minerals in Monterey Shale, Temblor Range, California. American Journal of Science 277:259-272.

Neumann M, Ehrmann W (2001) Mineralogy of sediments from CRP-3, Victoria Land Basin, Antarctica, as revealed by X-Ray Diffraction. Terra Antarctica 8:523-532.

Nolan M, Brigham-Grette J (2007) Basis hydrology, limnology, and meteorology of modern Lake El´gygytgyn, Siberia. Journal of Paleolimnology 37:17-35.

North Greenland Ice Core Project members: Andersen KK, Azuma N, Barnola JM, Bigler M, Biscave P, Caillon N, Chappellaz J, Clausen HB, Dahl-Jensen D, Fischer H, Flückiger J, Fritzsche D, Fujii Y, Goto-Azuma K, Grønvold K, Gundestrup NP, Hansson M, Huber C, Hvidberg CS, Johnson SJ, Jonsell U, Jouzel J, Kipfstuhl J, Landais A, Leuenberger M, Lorrain R, Masson-Delmotte V, Miller H, Motoyama H, Narita H, Popp T, Olander Rasmussen S, Raynaud D, Röthlisberger R, Ruth U, Samyn D, Schwander J, Shoji H, Siggard-Andersen

ML, Steffensen JP, Stocker T, Sveinbjörnsdottir AE, Svensson A, Takata M, Tison JL, Thortseinsson Th, Watanabe O, Wilhelms F, White JWC (2004) High-resolution record of Northern Hemisphere climate extending into the last interglacial period. Nature 431:147-151.

Nowaczyk N, Frederichs TW, Kassens H, Nøgaard-Pederson N, Spielhagen RF, Stein R, Weiel D (2001) Sedimentation rates in the Makarov Basin, central Arctic Ocean: a paleomagnetic and rock magnetic approach. Paleoceanography 16:368-389.

Nowaczyk N, Minyuk P, Melles M, Brigham-Grette J, Glushkova O, Nolan M, Loozhkin AV, Stetsenko TV, Andersen PM, Forman SL (2002) Magnetostratigraphic results from impact crater Lake El´gygytgyn, northeastern Siberia: a 300 kyr long high-resolution terrestrial palaeoclimatic record from the Arctic. Geophysical Journal International 150:109-126.

Nowaczyk N, Melles M, Minyuk P (2007) A revised age model for core PG1351 from Lake El´gygytgyn, Chukotka, based on magnetic susceptibility variations tuned to northern hemisphere insolation variations. Journal of Paleolimnology 37:65-76.

Osinski GR, Spray JG, Lee P (2001) Impact-induced hydrothermal activity within the Haughton impact structure, arctic Canada: Generation of a transient, warm, wet oasis. Meteoritics & Planetary Science 36:731-745.

Osinski GR, Lee P, Parnell J, Spray JG, Baron M (2005) A case study of impact-induced hydrothermal activity: The Haughton impact structure, Devon Island, Canadian High Arctic. Meteoritics & Planetary Science 40:1859-1877.

Overpeck JT, Sturm M, Francis JA, Perovich DK, Serreze MC, Benner R, Carmack EC, Chapin III FS, Gerlach SC, Hamilton LC, Hinzman LD, Holland M, Huntington HP, Key JR, Lloyd AH, MacDonald GM, McFadden J, Noone D, Prowse TD, Schlosser P, Vörösmarty C (2005) Arctic system on trajectory to new, seasonally ice-free state. EOS 86:309-313.

Pironon J, Pelletier M, de Donato P, Mosser-Ruck R (2003) Characterization of smectite and illite by FTIR spectroscopy of interlayer NH_4^+ cations. Clay Minerals 38:201-211.

Prokopenko AA, Hinnov LA, Williams DF, Kuzmin MI (2006) Orbital forcing of continental climate during the Pleistocene: a complete astronomically tuned climatic record from Lake Baikal, NE Siberia. Quaternary Science Reviews 25:3431-3457.

Prokopenko AA, Bezrukova EV, Khursevich GK, Solotchina EP, Kuzmin MI, Tarasov PE (2010) Climate in continental interior Asia during the longest interglacial of the past 500000 years: the new MIS 11 records from Lake Baikal, SE Siberia. Climate of the Past 6:31-48.

Raymo ME, Grant B, Horowitz M, Rau GH (1996) Mid-Pliocene warmth: stronger greenhouse and stronger conveyor. Marine Micropaleontology 27:313-326.

Raynaud D, Barnola JM, Souchez R, Lorrain R, Petit JR, Duval P, Lipenkov VY (2005) The record for marine isotopic stage 11. Nature 436:39-40.

Reeves JB III, McCarty GW, Reeves VB (2001) Mid-infrared diffuse reflectance spectroscopy for the quantitative analysis of agricultural soils. Journal of Agricultural and Food Chemistry 49:766-772.

Reeves JB III (2003) Mid-infrared diffuse reflectance spectroscopy: is sample dilution with KBr necessary, and if so when? American Laboratory 35:24-28.

Rice SB, Freund H, Huang WL, Clouse JA, Isaacs CM (1995) Application of Fourier transform infrared spectroscopy to silica diagenesis: the opal-A to opal-CT transformation. Journal of Sedimentary Research A65:639-647.

Rickert D, Schlüter M, Wallmann K (2002) Dissolution kinetics of biogenic silica from the water column to the sediments. Geochimica et Cosmochimica Acta 66:439-455.

Rodgers KA, Browne PRL, Buddle TF, Cook KL, Greatrex RA, Hampton WA, Herdianita NR, Holland GR, Lynne BY, Martin R, Newton Z, Pastars D, Sannazarro KL, Teece CIA (2004) Silica phases in sinters and residues from geothermal fields of New Zealand. Earth-Science Reviews 66:1-61.

Rosén P, Persson P (2006) Fourier-transform infrared spectroscopy (FTIRS), a new method to infer past changes in tree-line position and TOC using lake sediment. Journal of Paleolimnology 35:913-923.

Rosén P, Vogel H, Cunningham L, Reuss N, Conley DJ, Persson P (2010) Fourier transform infrared spectroscopy, a new method for rapid determination of total organic and inorganic and biogenic silica concentration in lake sediments. Journal of Paleolimnology 43:247-259.

Schmidt M, Botz R, Rickert D, Bohrmann G, Hall SR, Mann S (2001) Oxygen isotope of marine diatoms and relations to opal-A maturation. Geochimica et Cosmochimica Acta 65:201-211.

Schwammborn G, Federov G, Schirrmeister L, Meyer H, Hubberten H (2007) Periglacial sediment variations controlled by Late Quaternary climate and lake level rise at Elgygytgyn Crater, Arctic Sibiria. Boreas DOI 10.1111/j.1502-3885.2007.00011.x.

Siebielec G, McCarty GW, Stuczynski TI, Reeves JB III (2004) Near- and mid-infrared diffuse reflectance spectroscopy for measuring soil metal content. Journal of Environmental Quality 33:2056-2069.

Sifeddine A, Fröhlich F, Fournier M, Martin L, Servant M,Soubiès F, Turcq B, Suguio K, Volkmer-Ribeiro C (1994) La sedimentation lacustre indicateur de changements des paléoenvironnements au cours des 30 000 dernières années (Carajasm Amazonie, Brésil) [Lacustrine sedimentation as indicator of environmental change during the past 30 000 years (Carajas, Amazon, Brazil)] Comptes rendus de l´Académie des sciences 318(Series II):1645-1652.

Thiede J, Winkler A, Wolf-Welling T, Eldholm O, Myhre AM, Baumann KH, Henrichs R, Stein R (1998) Late Cenozoic history of the Polar North Atlantic: results from ocean drilling. Quaternary Science Reviews 17:185-208.

Twardowski J, Anzenbacher P (1994) Raman and IR spectroscopy in biology and biochemistry. Ellis Horwood, New York, London, Toronto, Sydney, Tokyo, Singapore.

Vogel H, Rosén P, Wagner B, Melles M, Persson P (2008) Fourier transform infrared spectroscopy, a new cost-effective tool for qualitative analysis of biogeochemical properties in long sediment records. Journal of Paleolimnology 40:689-702.

White WB (1974) The carbonate minerals. In: Farmer VC (ed.) The infrared spectra of minerals. Mineralogical Society Monograph 4, Adlard & Son, Dorking, Surrey, pp 227-284.

Wirrmann D, Bertaux J, Kossoni A (2001) Late Holocene paleoclimatic changes in western central Africa inferred from mineral abundance in dated sediments from Lake Ossa (Southwest Cameroon). Quaternary Research 56:275-287.

Annex

The following tables are available on the accompanying CD-ROM:

Table A.1 Conventionally measured biogeochemical property concentrations for $TC_{(EA)}$, $TC_{(LA)}$, TOC, TIC, TN, and BSi of the calibration set.

Table A.2 Conventionally measured biogeochemical property concentrations for $TC_{(EA)}$, $TC_{(LA)}$, TOC, TIC, TN, and BSi of the validation set.

Table A.3 Biogeochemical property concentrations for $TC_{(EA)}$, $TC_{(LA)}$, TOC, TIC, TN, and BSi of the validation set inferred by using FTIRS models based on sediments of the composite profile D1.

Table A.4 Biogeochemical property concentrations for TC, TOC, TN, and BSi of the validation set inferred by using FTIRS models based on sediments of core Lz1024.

Table A.5 FTIRS-inferred biogeochemical property concentrations for $TC_{(EA)}$, $TC_{(LA)}$, TOC, TIC, TN, and BSi of the core section related to MIS 11.

Table A.6 FTIRS-inferred biogeochemical property concentrations for $TC_{(EA)}$, $TC_{(LA)}$, TOC, TIC, TN, and BSi of the composite profile D1 (calibration set and validation set).